

Deviations from Arrhenius dynamics in high temperature liquids, a possible collapse, and a viscosity bound

Jing Xue¹, Flavio S. Nogueira², K. F. Kelton^{1,3} and Zohar Nussinov^{1,4}

¹*Department of Physics, Washington University, St. Louis, Missouri 63160, USA*

²*Institute for Theoretical Solid State Physics, IFW Dresden, Helmholtzstr. 20, 01069 Dresden, Germany*

³*Institute of Materials Science and Engineering, Washington University, St. Louis, Missouri 63130, USA*

⁴*Rudolf Peierls Centre for Theoretical Physics, University of Oxford, Oxford OX1 3PU, United Kingdom*



(Received 23 August 2021; accepted 29 September 2022; published 19 October 2022)

Liquids realize a highly complex state of matter in which strong competing kinetic and interaction effects come to life. As such, liquids are, generally, more challenging to understand than either gases or solids. In weakly interacting gases, the kinetic effects dominate. By contrast, low temperature solids typically feature far smaller fluctuations about their ground state. Notwithstanding their complexity, with the exception of quantum fluids (e.g., superfluid helium) and supercooled liquids (including glasses), various aspects of common liquid dynamics such as their dynamic viscosity are often assumed to be given by rather simple, Arrhenius-type, activated forms with nearly constant (i.e., temperature independent) energy barriers. In this paper, we analyze experimentally measured viscosities of numerous liquids far above their equilibrium melting temperature to see how well this assumption fares. We find, for the investigated liquids, marked deviations from simple activated dynamics. Even far above their equilibrium melting temperatures, as the temperature drops, the viscosity of these liquids increases more strongly than predicted by activated dynamics dominated by a single uniform energy barrier. For metallic fluids, the scale of the prefactors of the best Arrhenius fits for the viscosity is typically consistent with that given by the product (nh) with n the number density and h Planck's constant. More generally, in various fluids (whether metallic or nonmetallic) that we examined, (nh) constitutes a lower bound scale on the viscosity. We find that a scaling of the temperature axis (complementing that of the viscosity) leads to a partial collapse of the temperature dependent viscosities of different fluids; such a scaling allows for a functional dependence of the viscosity on temperature that includes yet is far more general than activated Arrhenius form alone. We speculate on relations between non-Arrhenius dynamics and thermodynamic observables.

DOI: [10.1103/PhysRevResearch.4.043047](https://doi.org/10.1103/PhysRevResearch.4.043047)

I. INTRODUCTION

The Arrhenius equation [1–5] is an empirical relation describing the relationship between the reaction rate and the temperature T of a chemical reaction [6,7]. The reaction rate constant $k(T)$ quantifies the speed at which the reaction occurs. The Arrhenius equation asserts that

$$k(T) \propto e^{-E_a/k_B T}. \quad (1)$$

Here, E_a is an “activation energy”, and k_B is the Boltzmann constant. Another expression, commonly derived in transition rate theory textbooks, the Eyring equation [8], contends that the transition rate is, more precisely, given by

$$k(T) = \frac{\kappa k_B T}{h} e^{-\Delta G/k_B T}. \quad (2)$$

In Eq. (2), the constant κ is the “transition coefficient” and h is Planck's constant. Similar to the Arrhenius equation [Eq. (1)],

the reaction rate in Eq. (2) depends exponentially on the Gibbs free energy of activation ΔG —which assumes the role of a barrier. This free energy barrier $\Delta G = \Delta H - T\Delta S$ generally includes both entropic (ΔS) and enthalpic (ΔH) contributions [9]. A weakly temperature dependent ΔG qualitatively emulates a dominant exponential decay [Eq. (1)] with a constant E_a . In the current paper, we will synonymously use E_a and ΔG to denote the effective (free) energy activation barriers. Related transition state forms have been posited over the years [6,7].

Beyond its historical roots in chemical reaction rates, the Arrhenius equation has seen widespread use in other (at times, interrelated) arenas including (i) semiconductor physics (e.g., where it enables a determination of the number of thermally activated electrons in the conduction and valence bands) [10] aiding theoretical design and enabling a basic understanding of diodes, transistors, solar cells, and other semiconductor devices, (ii) metallurgy (e.g., creep rate and the number of vacancies/interstitial sites in a crystal), e.g., [11–14], (iii) the analysis of data from dynamical probes such as those of dielectric response, NMR and NQR in a host of systems, e.g., [15–19], (iv) relaxation rates associated with particles of fixed structural “softness” (an analog of elastic defect density in amorphous systems whose average value correlates with the

Published by the American Physical Society under the terms of the [Creative Commons Attribution 4.0 International](https://creativecommons.org/licenses/by/4.0/) license. Further distribution of this work must maintain attribution to the author(s) and the published article's title, journal citation, and DOI.

viscosity) [20] and, notably, (v) fluid dynamics—the focus of our paper.

Before proceeding further, we must briefly comment on a well known exception to activated liquid dynamics—that of supercooled fluids, e.g., [21–34]. Compounding the silicates that have been known to form glasses since antiquity, numerous liquids may be experimentally supercooled below their “freezing” or liquidus temperature T_l . Such a rapid cooling does not enable the liquids to change their phase and thus crystallize at the equilibrium freezing temperature. At low enough temperatures, these supercooled liquids assume a glassy amorphous state. During the supercooling process, the typical relaxation time scale of the liquids may increase dramatically by many orders of magnitude for a modest temperature drop and strongly deviate from the Arrhenius form of Eq. (1). This capricious divergence from activated dynamics is one of the principle features underscoring the enigmatic character of supercooled liquids and glasses.

Excusing the above celebrated exception of supercooled liquids as well as that of quantum fluids at cryogenic temperatures (most notably, low temperature Helium at ambient pressure), the viscosity η of most equilibrated liquids (including glass formers at sufficiently high temperatures above their liquidus temperature) has, for decades, been largely presumed to be given by an Arrhenius type expression. Specifically, it is commonly assumed that the typical relaxation time τ of liquids is given by

$$\tau = \tau_0 e^{E/T}. \quad (3)$$

In Eq. (3), the activation barrier E_a has been rescaled by the Boltzmann constant k_B so that it is measured in units of temperature (Kelvin) (i.e., $E \equiv E_a/k_B$). While in harmonic solids, there is a linear (Hooke law like) relation between stress and strain, in fluids, it is the strain rate [the time derivative of the strain (or displacement)] that is linearly proportional to the stress (or force); this is a continuum counterpart to the linear relation between the applied force and particle velocity in a viscous system (with the ratio between the two being set by a viscosity). By the Maxwell model for viscoelasticity, the dynamic viscosity scales as

$$\eta = \mathbf{G}\tau, \quad (4)$$

where \mathbf{G} is the instantaneous shear modulus [28] and τ is the relaxation time (inverse strain relaxation rate). Typically, \mathbf{G} has a much more mild temperature dependence than that of the relaxation time. From these and other considerations, viscosities are often anticipated to display a behavior similar to that of Eq. (3),

$$\eta(T) = \eta_0 e^{E'/T}. \quad (5)$$

Indeed, e.g., aside from Eq. (3), also the Eyring form of Eq. (2) leads, in certain treatments [8,29] to Eq. (5) with a viscosity prefactor η_0 that scales with the particle number density n (a quantity that is, typically, weakly temperature dependent). Thus, on the whole, the time scale governing liquid dynamics and the respective viscosities are often assumed to be effectively governed by a single activation barrier of uniform height that is set by E and with a constant prefactor η_0 . Equation (5) was first noted in a paper by Reynolds [35] (three years before Arrhenius introduced his now famous

equation for reaction rates). Nonetheless, viscosity satisfying Eq. (5) is commonly said to be of the “Arrhenius” type due to the intuitive connection, briefly reviewed above, that the Arrhenius rate equation of Eq. (1) evokes. In the many years since, this relation has been posited and rediscovered anew by several researchers (perhaps most notably, by Guzman [36] and Andrade [37] [in some circles, Eq. (5) is known as the Guzman-Andrade or Andrade equation]).

In the current paper, we will extensively analyze the temperature dependence of the dynamic viscosities of numerous fluids. Empirically, in accord with certain theoretical anticipations [related to those underlying Eq. (2)], when fitting the viscosities of various fluids to the Arrhenius form of Eq. (1), the prefactor in Eq. (5) (η_0) was, in certain instances, found to be of the scale of a particularly simple product: (nh) . Here, h is Planck’s constant and n denotes the number of particles per unit volume [8,29,30,38,39]. In a more general vein, the product (nh) has thus been suggested to be a lower bound on the scale of the viscosity [29]. (A related tighter bound differing by factors of mass ratios was later proposed in [40].) In the current paper, we will demonstrate that empirically

$$\eta \geq \mathcal{O}(nh). \quad (6)$$

Related lower bounds on the viscosity were further rigorously proven in [41].

Low viscosity is associated with a high Reynolds number regime where the system may become most turbulent. In conventional materials, the viscosity is minimal at a crossover between the gaseous and fluid viscosity behaviors. In the gas (due to increased collisions between the molecules as the gas is heated and thus an effective increase in the coupling between layers), the viscosity increases with temperature. By contrast, in the fluid, the viscosity monotonically drops with temperature due to increased thermal motion, which effectively reduces the coupling between fluid layers (the interactions become less important relative to thermal effects). Fluids with high viscosity support laminar flow wherein shear stresses readily dampen applied perturbations. The two opposing behavioral trends of monotonic decrease and increase in the viscosity as a function of temperature in, respectively, the fluid and the gas mandate an experimentally observed intervening viscosity minimum [that, as noted above, empirically satisfies Eq. (6)].

Broader than the single uniform activation barrier of Eq. (5), any function $\eta(T)$ may be written as a Laplace transform in the inverse temperature $\beta = \frac{1}{T}$ (after, once again, rescaling the activation energies by k_B) via a distribution $P(E')$ of effective energy barriers,

$$\frac{1}{\eta(T)} = \frac{1}{\eta_0} \int P(E') e^{-\frac{E'}{T}} dE'. \quad (7)$$

As Eq. (7) emphasizes, in principle, an inverse Laplace transform of any data set over an extensive range of temperatures will trivially yield an activation energy distribution P . This distribution will, by construction, reproduce the measured viscosity data. Physically, the distribution P may be not only a function of the activation energy alone but also of the temperature. In a similar spirit, for the viscosity data of liquids below their liquidus temperature T_l (not above it as we focus on in the current paper), a particular theory [23–26] repro-

duces all experimentally measured data of supercooled liquids over 16 decades of viscosity with a single-parameter scale free temperature-dependent normal distribution P of effective equilibrium relaxation rates. In what follows, we will test the applicability of Eq. (7) with a delta function distribution $P(E') = \delta(E - E')$ associated with the commonly assumed activation energy form of Eq. (5) for high temperature liquids (above their melting temperature). Throughout this paper, *all values of the dynamic viscosity η (as well as the scale η_0) will be quoted in units of $\text{Pa} \cdot \text{s}$ ($= 0.1$ Poise).* In order to provide an everyday intuitive feel for these conventional units, we remark that the viscosity of water at room temperature is ~ 1 centiPoise = milli- $\text{Pa} \cdot \text{s}$. While numerous investigations applied the fit of Eq. (5) for the dynamic viscosities to various fluids, we are not aware of much work that critically focused on and tested the veracity of the Arrhenius form to these viscosities and any deviations thereof. It is important to underscore that, notwithstanding their simple intuitive appeal, there are no rigorous derivations of activated dynamics in fluids. Indeed, theoretically determining the viscosity of fluids as a function of their temperature is not, at all, an easy problem. Unlike the solid (where interaction effects dominate) or the gas (where kinetic effects are important), in the fluid, both kinetic effects and interactions are comparable and compete with one another. In this paper, we will test the validity of Arrhenius form of equilibrium fluids (at temperatures $T > T_f$). Towards this end, we will compute, within various temperature intervals, values of effective activation energy E and prefactor η_0 that match the experimental values of the viscosity when Eq. (5) is assumed. These tests will enable us to comment on the high temperature limits of various well known fits to the viscosity of glass forming liquids, e.g., [38,42–45]. Various notable works advanced and tested various (kinematic) viscosity fits, e.g., [46]. To our knowledge, there are no prior investigations explicitly focusing on the effective activation energies associated with high temperature liquids.

In the current paper we will frequently refer to *two different temperatures*:

(1) In several earlier studies of glass forming fluids, e.g., the above noted [38,42–44], a *crossover temperature* T_A was identified below which ($T < T_A$) strong deviations from Arrhenius behavior were found and above which (temperatures $T > T_A$) the dynamics seemed to conform to an approximate Arrhenius form.

As we will detail, our analysis reveals that, as a general trend, even up to temperatures far above melting, disparate fluids may exhibit a viscosity that varies more significantly with temperature than activated dynamics [Eq. (5)] would predict. In other words, the commonly assumed simple Arrhenius form does not, in fact, accurately capture fluid dynamics. Towards that end,

(2) We tested for a *broader temperature dependence* associated with a *general scaling temperature* T_{sc} . Specifically, we examined whether scaled dimensionless viscosities of different fluids η/η_0 can, in their high temperature regime, be made to collapse as a function of corresponding dimensionless inverse temperatures T_{sc}/T . Here, η_0 and T_{sc} are fluid specific parameters. The Arrhenius form of Eq. (5) is only one realization of such a possible collapse; in the Arrhenius form, the activation energy E is set by T_{sc} and the function

specifying the associated collapse is the exponential function. We searched for such a more general possible collapse and determined the optimal associated temperature scales T_{sc} over a broad range of viscosities. Our tests revealed that certain fluids exhibit nearly identical dependencies on the temperature over 13 decades of viscosity while others collapse over a far more limited range.

II. OUTLINE

The remainder of this article is organized as follows. We begin, in Sec. III, by describing simple litmus tests indicating deviations from Arrhenius dynamics with constant activation energies. We then turn (Sec. IV) to briefly discuss the various fluids that we analyzed and the smoothening procedure invoked in our numerically evaluated derivatives. Sections V, VI, and VII quantify, via complementary calculations, the deviations from simple Arrhenius dynamics. Taken together, these analyses illustrate how the effective activation barriers typically increase as the temperature is lowered. In Sec. VIII, we demonstrate that it is possible to collapse the viscosity data from different fluids onto a curve with some liquids persisting for many decades of the viscosity for while others such a collapse is over a very limited range. In Sec. IX, we illustrate that the lower bound [29] on the viscosity of Eq. (6) holds for all materials investigated and contrast it with other more recent proposed bounds [40]. We conclude with a synopsis of our results in Sec. X. Various technical details have been relegated to the Appendices.

III. HALLMARKS OF DEVIATIONS FROM SIMPLE ACTIVATED DYNAMICS IN EQUILIBRATED HIGH TEMPERATURE FLUIDS

Since the viscosity of various fluids typically span several decades as their temperature is varied, we will analyze Eq. (5) on a logarithmic scale,

$$\ln \eta(T) = \ln \eta_0 + \frac{E}{T}. \quad (8)$$

We now explicitly highlight the exceedingly simple principles underlying much of our study. If Eq. (8) holds, then both E and η_0 as adduced from (numerical) derivatives of the experimentally measured viscosities of all studied liquids should be temperature independent constants. That is, for simple activated dynamics, both

$$E = \frac{d}{d(1/T)} \ln \eta \quad (9)$$

and

$$\ln \eta_0 = \frac{d}{dT} (T \ln \eta) \quad (10)$$

must, for each individual fluid, assume the same value at all temperatures. Temperature variations of the derivatives of Eqs. (9) and (10), if any exist, will attest to the degree to which departures from the putative Arrhenius form of Eq. (5) appear.

Given the above corollaries for temperature independent E and η_0 as determined from derivatives, we display in Fig. 1 (see left-vertical axis) our approximate numerical for the activation energy of Eq. (9) as deduced from experimentally

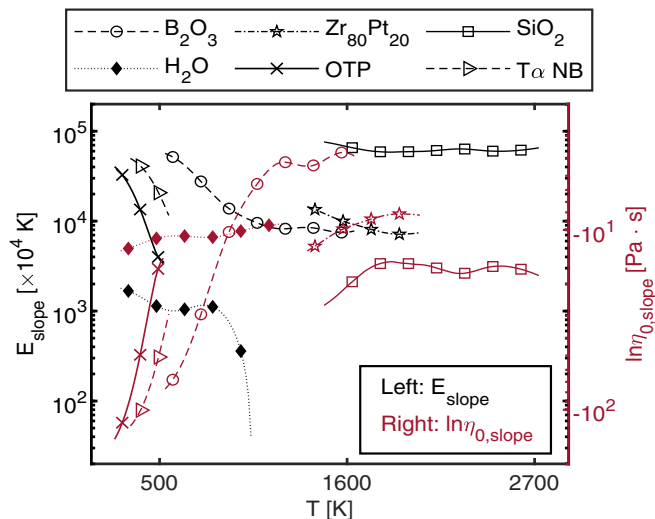


FIG. 1. Finite difference numerical (“slope”) approximations of the effective activation energy E of Eq. (9) (as determined by the finite gradient approximation of Eq. (13), see left-vertical axis with points marked in black) and of η_0 of Eq. (10) (as computed via the finite difference approximation of Eq. (14), see right-vertical axis with points highlighted in red) for six liquids above their liquidus temperature T_l . Notwithstanding fluctuations, it is seen that across all fluids, as the temperature decreases, the finite difference approximation to the effective activation energy $E(T)$ becomes larger. The “strong” glass forming fluid SiO_2 [47] exhibits a nearly constant large effective energy barrier at the high temperature shown (far above that of supercooling and glass formation). The finite difference approximations to η_0 as computed from Eq. (10) increase as temperature rises. Combined with their more notable deviations from Arrhenius dynamic, the sparse viscosity data of B_2O_3 , OTP, and $T\alpha\text{NB}$ give rise to curves that are not very smooth.

measured viscosities for all liquids, which we analyzed above their liquidus (or melting) temperature T_l . Similarly, on the right-vertical axis of Fig. 1, we provide our numerically evaluated results for Eq. (10) at temperatures about the equilibrium liquidus temperature.

As Fig. 1 makes evident, empirical numerical approximations to the derivatives of Eqs. (9) and (10) are not temperature independent constants. Specifically, as Fig. 1 attests for temperatures $T > T_l$ (and, respectively, Figs. 9 and 10 in Appendix B demonstrates for $T > T_{sc}$), at the lower end of the temperature range (and usually at far higher temperatures as well):

The effective activation energy as computed from Eq. (9) increases significantly as the temperature T decreases.

In order to quantitatively contrast the viscosity with the ansatz of Eq. (5) with empirical results, we may endow $\eta_0 \rightarrow \eta_0(T)$ and/or $E \rightarrow E(T)$ with temperature dependencies so as to optimally fit the experimental viscosity data. (Varying any one of these parameters alone will suffice to fit any experimental data set.) By fiat, the activated form of Eq. (5) assumes the absence of any such temperature dependencies. If Eq. (5) applies, with moderate variations of $E(T)$ and $\eta_0(T)$, then (since η is exponential in E) a numerical evaluation of Eq. (10) will capture the derivative dE/dT of the effective activation barrier. The marked decrease of the numerically

evaluated Eq. (10) in Fig. 1 indicates that the rate of increase of the effective activation barrier $E(T)$ as the temperature T is decreased becomes more pronounced as the temperature is lowered. Similar trends (made evident in Fig. 10) are also visible at temperatures above the (typically) higher temperature crossover temperature T_A [38,42–45]. The astute reader may note from these figures that for water, at sufficiently high temperatures, some of these trends are reversed. This is so since the extended temperature range that we investigate also includes temperatures above the boiling point of water (373 K) where the system is no longer a liquid. Indeed, while an increase in temperature typically decreases the viscosity of the liquid, in a gas this trend is reversed.

Equation (8) is trivially invariant under the simultaneous transformations

$$\begin{aligned} \eta_0(T) &\rightarrow \eta_0(T)e^{-\frac{f(T)}{T}}, \\ E(T) &\rightarrow E(T) + f(T), \end{aligned} \quad (11)$$

with $f(T)$ an arbitrary function of the temperature. As further discussed in Appendix C, possible effective temperature dependencies of E and η_0 may be obtained by, e.g., explicitly plotting

$$T \ln \eta = T \ln \eta_0 + E \quad (12)$$

as a function of the temperature. The equality of Eq. (12) was implicitly invoked in deriving Eq. (10) under the assumption of constant E and η_0 . As seen from Eq. (12), if the ansatz of Eq. (5) applies, then a plot of $(T \ln \eta)$ as a function of T will yield a line with a slope set by $\ln \eta_0$ and intercept equal to E . Setting, in Eq. (11), $f = aT + b$ (with general constants a and b) to be an arbitrary linear function will yield other consistent parameters for any such nearly constant E and η_0 . Taken together, Eqs. (9), (10), and (12) [all which trivially stem from Eq. (8)] allow for an estimate of the typical values of E and η_0 . This will also allow us to monitor for any temperature variations from assumed constant values of these parameters. Detailed analyses of various high temperature fluids all lead to our earlier highlighted conclusion: If the viscosity of liquids is fitted to a single uniform activation energy form then the resulting $E(T)$ exhibits, on the whole, an increase as T is lowered.

In what follows, we briefly discuss the liquids that we examined and our discrete temperature difference approximations to the derivatives of Eqs. (9) and (10).

IV. THE STUDIED LIQUIDS AND GENERAL ASPECTS OF THE DATA ANALYSIS

We list all of the liquids that we study along with some of their properties (such as the scaling temperature T_{sc} , which we describe next) in Table I. Our focus is on high temperature behavior (i.e., at temperatures far above the liquidus temperature) where Arrhenius behavior was assumed to universally hold for all liquids. The liquids in Table I include good glass forming liquids known to display non-Arrhenius dynamics when supercooled to temperatures lower than T_l . For the metallic fluid glassformers [48], plots of $\ln(\eta/\eta_0)$ as a function of T_{sc}/T , with a material dependent T_{sc} for each individual fluid, collapse onto a single universal curve [38].

TABLE I. Measurements of liquidus temperature T_l , crossover temperature T_{sc} by us and T_A from previous published paper [38], $\ln \eta_0$ and $\ln(nh)$ (both are measured in $Pa \cdot s$) [38]. For metallic liquids, their η_0 is nearly equal to their nh value [see Eq. (15)]. By contrast, the liquids H_2O and B_2O_3 have η_0 values that are much smaller than their respective nh values. The error bar of T_{sc} is 1K while the error bar of $\ln \eta_0 [Pa \cdot s]$ is 0.001. The method of determining T_{sc} (and thus also the corresponding $\ln \eta_0$) is provided in Fig. 2. Where the data was taken from sources other than our own measurements and/or [38], these have been cited below. The data of H_2O have been calibrated by combining [40,50]. The column marked “TB bound” is a lower bound on $\ln \eta$ [40], which we will return to in Sec. IX. When the parameters were unknown they were left blank.

Composition	T_l [K]	T_{sc} [K]	T_A [K]	$\ln \eta_0$ [Pa · s]	$\ln(nh)$ [Pa · s]	TB bound [Pa · s]	Density at T_l [g/cm ³]
Cu ₄₃ Zr ₄₅ Al ₁₂	1209	1371		-10.829			
Cu ₄₆ Zr ₅₄	1198	1212		-10.601			
Cu ₄₇ Zr ₄₅ Al ₈	1190	1345		-10.868			
Cu ₄₇ Zr ₄₇ Al ₆	1172	1307		-10.756			6.83
Cu ₄₉ Zr ₄₅ Al ₆	1177	1324		-10.945			
Cu ₅₀ Zr ₄₀ Ti ₁₀	1168	1276		-10.877			6.90
Cu ₅₀ Zr _{42.5} Ti _{7.5}	1152	1237		-10.903			6.92
Cu ₅₀ Zr ₄₅ Al ₅	1173	1329	1308	-10.879	-10.2258	-6.3847	6.91
Cu ₅₀ Zr ₅₀	1226	1273	1284	-10.831	-10.2419	-6.3796	
Cu ₅₃ Zr ₄₅ Al ₂	1199	1290		-10.915			
Cu ₅₅ Zr ₄₅	1193	1298		-11.003			
Cu ₆₀ Zr ₂₀ Ti ₂₀	1127	1302	1301	-11.174	-10.0991	-6.3168	6.92
Cu ₆₀ Zr ₄₀	1168	1275		-10.893			
Cu ₆₄ Zr ₃₆	1230	1320		-11.139			
LM601	1157	1318		-10.588			
Ni _{59.5} Nb _{40.5}	1448	1637		-10.479			
Ti _{38.5} Zr _{38.5} Ni ₂₁		1277		-10.8			
Ti ₄₀ Zr ₁₀ Cu ₃₀ Pd ₂₀	1189	1297	1299	-10.901	-10.1521		6.82
Ti ₄₀ Zr ₁₀ Cu ₃₆ Pd ₁₄	1185	1274	1278	-10.952	-10.1360	-6.3689	6.69
Vit105	1093	1369		-10.618			6.46
Vit106	1123	1362	1373	-10.505	-10.3156		6.44
Vit106a	1125	1357	1360	-10.646	-10.3156		6.51
Zr ₅₇ Ni ₄₃	1450	1342		-10.414			
Zr ₅₉ Ti ₃ Ni ₈ Cu ₂₀ Al ₁₀	1145	1313.5		-10.691	-10.3547		6.41
Zr ₆₀ Ni ₂₅ Al ₁₅	1248	1395	1421	-10.516	-10.3662		6.23
Zr ₆₂ Cu ₂₀ Ni ₈ Al ₁₀	1152	1321	1325	-10.531	-10.3639	-6.5063	
Zr ₆₄ Ni ₂₅ Al ₁₁	1212	1350		-10.394			
Zr ₆₄ Ni ₃₆	1283	1256	1223	-10.27	-10.3271	-6.4512	
Zr ₆₅ A _{7.5} Cu _{17.5} Ni ₁₀	1170	1267		-10.274			6.5
Zr ₇₄ Rh ₂₆	1350	1357		-10.144			
Zr _{75.5} Pd _{24.5}	1303	1289		-10.284			
Zr ₇₆ Ni ₂₄	1233	1157	1161	-10.057	-10.4123	-6.5125	
Zr ₈₀ Pt ₂₀ [38,58]	1450	1482	1549	-10.004	-10.3939	-6.3468	8.38
H ₂ O [40,50]	273.15	297		-13.4	-10.7181	-9.6671	0.997
B ₂ O ₃ [51]	723	1187		-4.289	-11.1740	-9.8872	2.460
OTP [52]	330	411		-13.05			
T α NB [52]	435	652		-13.5			
SiO ₂ [53]	1986	3455		-3.4	-11.136	-9.7028	2.65

Figure 2 shows both the raw and filtered data of Zr₈₀Pt₂₀ and the corresponding fit of Eq. (5). By “filtered data”, we refer to the replacement of $\ln \eta(T)$ by the average of $\ln \eta(T)$ over a finite temperature window $[T - \frac{\Delta T}{2}, T + \frac{\Delta T}{2}]$ centered about each temperature T . Averages over finite width (ΔT) temperature windows suppress oscillations of the raw empirical values of $\ln \eta(T)$. In Appendix E, we further discuss these averages. The linear fit in Fig. 2 illustrates how a crossover temperature T_A (and a scaling temperature T_{sc} for which such a collapse occurs) may be ascertained [49].

The values of $\ln \eta_0$ listed in Table I are those associated with the fit of Eq. (5) for temperatures $T < T_{sc}$. The viscos-

ity data of the metallic liquids were measured by one of us [30]. Other viscosity data were extracted by scanning graphs from published works [50–53]. The process of scanning and digitizing the experimental plots was performed with data digitalization software [54].

The viscosity data inherently display noise present in the original experiments and scanning errors. In order to reduce the noise, we applied equidistance interpolation to the data and designed a low-pass finite impulse response (FIR) filter [55–57] (see Appendix E). We then fitted the filtered data with Eq. (8) for all temperatures above the liquidus temperature

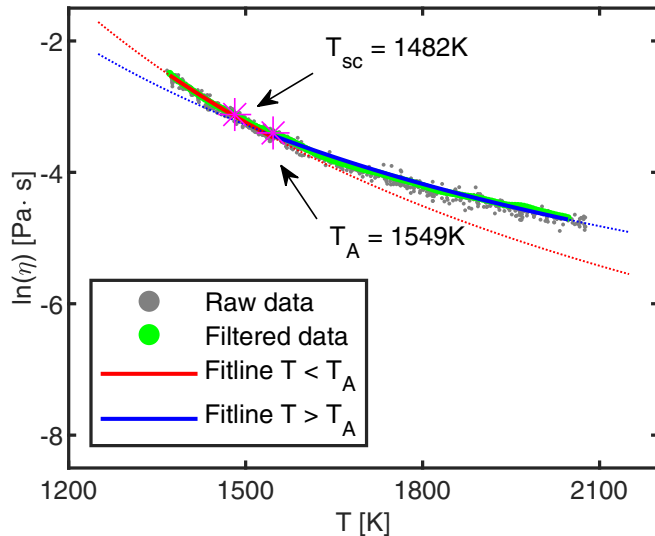


FIG. 2. The determination of a crossover temperature T_A [38,42–45]. A comparison of the temperature-dependent viscosity data for $Zr_{80}Pt_{20}$ and the Arrhenius form of Eq. (5). The gray dots represent the raw experimental data; the green curve marks the “filtered” data (i.e., the data averaged over a fixed temperature window to minimize the experimental noise). The solid-red line is a fit to Eq. (8) of the filtered data for temperatures $T > T_A$ (see [38,45] for the definition and discussion of T_A for general fluids), and the solid-blue line is for temperatures $T < T_A$. The dashed-red and blue lines are, respectively, extrapolated (Arrhenius type) curves of an effective constant activation energy. At higher temperatures (see the dashed-blue line), the deviations from the expected constant activation energy of Eq. (5) are not nearly as pronounced as those at lower temperatures (see the dashed-red line for temperatures $T < T_A$). Taken together, the latter curves point towards an approximate crossover from an effective Arrhenius behavior in the shown temperature range above T_A to a markedly non-Arrhenius one at lower temperatures. The temperature T_{sc} is the “scaling temperature” that is discussed in the main text.

T_l as well as the scaling temperature T_{sc} discussed in the Introduction.

V. EXTRACTING THE EFFECTIVE, TEMPERATURE DEPENDENT, ACTIVATION ENERGIES FROM NUMERICAL DERIVATIVES

Our filtered data are quite detailed with a minimal temperature interval $\Delta T = 0.25$ K between subsequent data points (labelled an index i). As briefly alluded to in Sec. III, this allows for numerical approximations of Eq. (9) via finite temperature differences,

$$E_{\text{slope}} = \frac{\ln \eta_{i+1} - \ln \eta_i}{1/T_{i+1} - 1/T_i}. \quad (13)$$

The finite difference approximation of Eq. (13) to the derivative of Eq. (9) is acutely sensitive to local variations of $\ln \eta$ as a function of the temperature. This drawback compounds the errors already present in the raw data. In order to see an intelligible trend, we apply a low-pass FIR filter (see Appendix E) to calculate E_{slope} . As an illustrative example, we consider several aspects of $Zr_{80}Pt_{20}$ in Figs. 3 and 4. The black curve in Fig. 4(a) represents the activation energy E as

obtained from Eq. (13) whereas the red curve is the resulting plot after applying the filter. We used this method to obtain E as a function of T above T_l as displayed in Fig. 1. (The analogous results for $T > T_{sc}$ appear in the Appendix (Fig. 9 and Fig. 10).)

VI. DETERMINING AN EFFECTIVE η_0 IN DIFFERENT TEMPERATURE WINDOWS FROM NUMERICAL DERIVATIVES

Assuming a constant activation barrier, an effective temperature dependent $\ln \eta_0$ may, as we discussed earlier, be computed via Eq. (10). Similar to Eq. (13), the derivative in Eq. (10) may be approximated by a finite difference gradient,

$$\ln \eta_{0,\text{slope}} = \frac{(T \ln \eta)_{i+1} - (T \ln \eta)_i}{T_{i+1} - T_i}. \quad (14)$$

The prefactor results of Fig. 1 for temperatures above the liquidus temperature T_l (and those of Fig. 10 of the Appendix for temperatures larger than a crossover temperature T_{sc}) illustrate, unambiguously, that the Arrhenius form does not hold. If E is kept fixed then the prefactor η_0 of Eq. (5) cannot be a temperature independent constant; in most liquids, the value of η_0 necessary to fit the data changes by several orders of magnitude.

In Fig. 3, we contrast the optimal values of the activation energy E_{avg} with E_{slope} [Eq. (13)] and the viscosity prefactor $\eta_{0,\text{avg}}$ with $\eta_{0,\text{slope}}$ of Eq. (14). Here, E_{avg} and $\eta_{0,\text{avg}}$ refer to the constant (temperature independent) values of the activation energy and viscosity prefactor in the Arrhenius expression for the viscosity that fit the data best. Details of the optimization procedure are given in Appendix A. As we noted above, according to theoretical (Eyring-type) predictions [8,29,30,38,39], the viscosity prefactor

$$\eta_0^{\text{theory}} = nh. \quad (15)$$

As we alluded to earlier, n denotes the number particle density and h is Planck’s constant. In Table I, we compare the found fitted values with the prediction of Eq. (15). While the discrepancy between the empirical value of η_0 and η_0^{theory} is relatively small for *metallic liquids* [29,38] [see also Fig. 3(a)], it can become far more marked for nonmetallic fluids fitted over a large temperature range [Figs. 3(b) and 3(c)]. The explicit functional form for the viscosity associated with the scaling temperature T_{sc} will be elaborated on in Eq. (18).

VII. EFFECTIVE ENTROPY

When employing the Eyring form of Eq. (2), if the Gibbs free energy barrier ΔG is almost constant then Arrhenius dynamics will appear. Our results establish, however, that the effective activation barrier (E_{slope}) required to conform the experimental data is clearly temperature dependent. Thus, if we attempt to describe the data with the Eyring equation that the effective Gibbs free energy barrier ΔG varies with temperature. Such a variation implies that the *effective entropy*

$$\Delta S \equiv -\left(\frac{\partial \Delta G}{\partial T}\right) \quad (16)$$

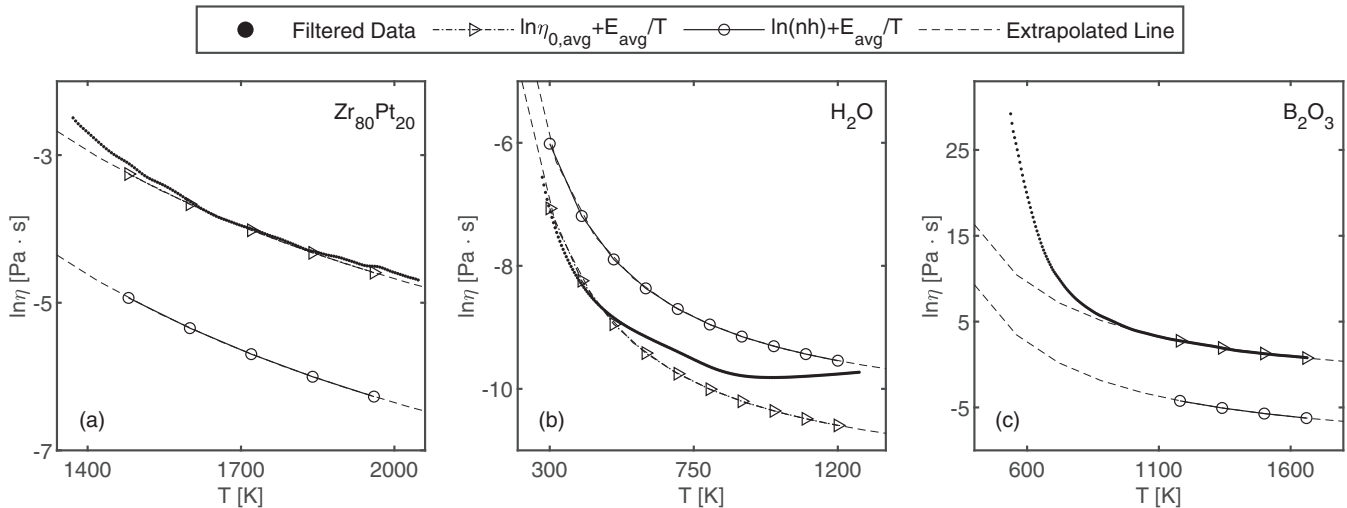


FIG. 3. Comparison between the measured viscosity of, $Zr_{80}Pt_{20}$, H_2O , and B_2O_3 with the Arrhenius form of Eq. (8) (see Sec. IX for further comparisons). The ordinate represents the natural logarithm of the numerical value of the viscosity η when the latter is measured in units of $Pa \cdot s$. In all panels, the black scatters refer to the filtered experimental $\ln \eta(T)$ data that are contrasted with the Arrhenius fits of Eq. (8). The line delineated by triangular markers is the Arrhenius fit of Eq. (8) obtained with an optimal uniform “average” (see Appendix A for details) activation energy E_{avg} with a viscosity prefactor $\ln \eta_{0,avg}$ values that fit the data well. The curve with circular markers represents the fit of Eq. (8) by setting $\ln \eta_0 = \ln(nh)$ where n is the number density and h is Planck’s constant. (Similar to the logarithm of the viscosity, $\ln(nh)$ denotes the natural logarithm of the numerical value of (nh) when (nh) is measured in units of $Pa \cdot s$.) The thin-dashed curves are extrapolations. (a) The filtered experimental data of $Zr_{80}Pt_{20}$ are compared with Arrhenius fits with $E_{avg} = 8080$ K, $\ln \eta_{0,avg} = -8.666$ and $\ln \eta_0 = \ln(nh) = -10.394$ for temperatures above $T_l = 1450$ K. (b) A comparison between the measured viscosity of H_2O with the Arrhenius fit of Eq. (8). An optimal fit for $T > T_l = 273.15$ K is obtained by setting $E_{avg} = 1411$ K, $\ln \eta_{0,avg} = -11.770$, and $\ln(nh) = -10.718$. (c) A comparison of B_2O_3 with $E_{avg} = 8189$ K, $\ln \eta_{0,avg} = -4.177$, and $\ln(nh) = -11.174$ for $T > T_l = 723$ K.

does not vanish. To ascertain the scale of this effective entropy, we may replace ΔG by E_{slope} and employ our finite temperature difference approximations (that we earlier invoked to determine E_{slope}) to rewrite Eq. (16),

$$\Delta S_{slope} = -\frac{E_{slope,i+1} - E_{slope,i}}{T_{i+1} - T_i}. \quad (17)$$

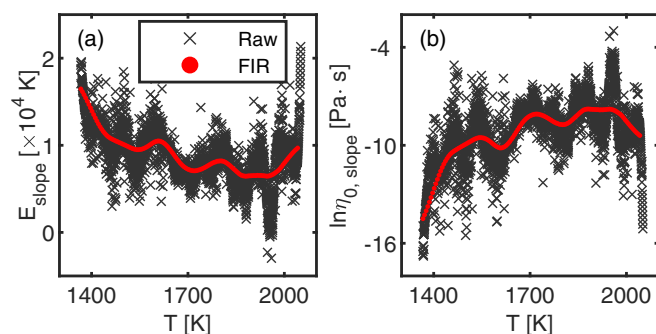


FIG. 4. (a) The effective activation energy E_{slope} of Eq. (13) for the metallic liquid $Zr_{80}Pt_{20}$. The black curve is the raw finite difference gradients [Eq. (13) as evaluated over temperature windows of width $(T_{i+1} - T_i)$ between consecutive points]. The red curve displays these finite difference gradients as smoothed via a finite impulse filter (FIR) (Appendix E). (b) The effective $\ln \eta_{0,slope}$ of the metallic liquid $Zr_{80}Pt_{20}$ as evaluated over different temperature windows. Similar to (a), the black curve provides the raw finite difference gradients of Eq. (14) represents $\ln \eta_{0,slope}$ while the red curve corresponds to a finite difference gradient generated by an FIR with a larger temperature window.

In Fig. 5, we display both the filtered and unfiltered results of ΔS_{slope} resulting from such finite temperature differences [with, in Eq. (17), the energies E_{slope} explicitly measured in Joules (i.e., not, as in much of this paper, rescaled by the k_B and represented as a temperature scale)] when examining $Zr_{80}Pt_{20}$. Employing a larger temperature interval ΔT avoids noise in the data and consistently yields positive effective entropy change ΔS . This effective entropy change underscores the deviation from Arrhenius dynamics with a constant effective energy barrier. The positive sign of ΔS highlights, once again, the monotonic variation of the effective activation barrier with temperature in the liquid phase. Performing a linear fit illustrates that, on average, the ascertained effective entropy ΔS_{slope} monotonically rises with increasing temperature. The latter further implies an average positive “effective heat capacity” $C_{eff} \equiv T \frac{\partial \Delta S}{\partial T}$.

VIII. TESTS OF A MORE GENERAL UNIVERSAL VISCOSITY COLLAPSE

Having established that viscosities may, generally, be far more complex than simplest activated functions of the temperature, we now ask whether more general scaling forms may better fit the data. That is, we will now inquire whether hallmarks of the commonly assumed universal (activated) dynamics may be seen by broader tests. To achieve this goal, we critically tested if $\eta(T)/\eta_0$ might be another (not necessarily the simple exponential appearing in the Arrhenius equation) universal function F of a dimensionless temperature T_{sc}/T with both η_0 and the scaling temperature T_{sc} being specific constants for each fluid. If such a universal function exists then

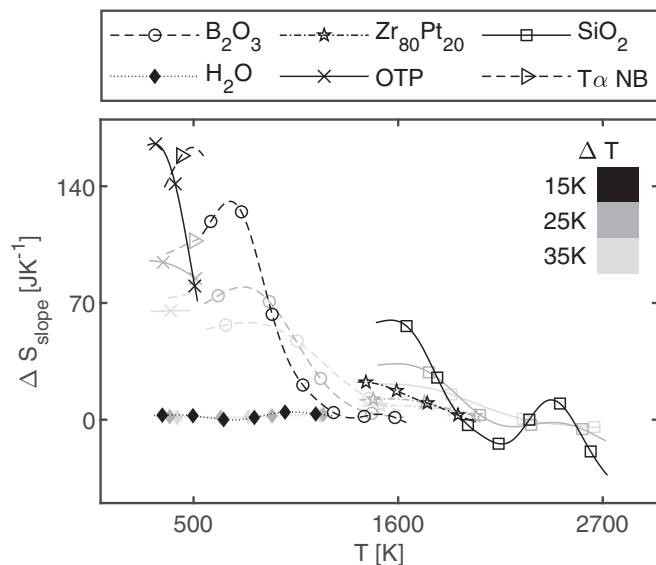


FIG. 5. The effective entropy ΔS_{slope} defined by Eq. (17) for selected liquids above their liquidus temperature T_l . The finite difference gradients of Eq. (17) are evaluated over consecutive temperature windows (i) of width $(T_{i+1} - T_i)$. Excusing fluctuations in the numerical data, the effective activation barrier generally decreases with increasing T . Thus, when computing numerical differences over a larger temperature interval, the average effective entropy as computed by Eq. (17) is positive. As the color bar indicates, the black curves are all defined by Eq. (17) at temperature interval $\Delta T = 15$ K, and the gray and light-gray curves are similarly computed for, respectively, $\Delta T = 25$ K, 35 K.

plotting, for N disparate liquids, the dimensionless viscosity η/η_0 as a function of the dimensionless temperature T_{sc}/T (with T_{sc} replacing the activation barrier E of the Arrhenius form) will lead to curve whose form is given by the aforementioned universal function F . As is well known, when present, a data collapse onto a universal curve underscores an underlying simplicity. The celebrated Guggenheim fit [59] first illustrated that the scaled dimensionless densities of various liquids in the vicinity of their critical points are a universal function of scaled dimensionless reduced temperatures. Guggenheim reported on this data collapse onto a universal curve long before the current advent of critical phenomena [60]. Inspired by these well known results, we assess to what extent a collapse might or might not occur for the viscosities of various fluids with such liquid dependent adjustable temperature (T_{sc}) and viscosity (η_0) scales,

$$\frac{\eta}{\eta_0} = F\left(\frac{T_{sc}}{T}\right). \quad (18)$$

Here the function $F(z)$ will not be constrained to the exponential function (e^{cz} with c a constant) defining the Arrhenius form of Eq. (5). Operationally, we adjust the constants T_{sc} and η_0 such that, the scaled curves of $\ln(\eta/\eta_0)$ as a function of T_{sc}/T of the different fluids enjoy a large overlap. Earlier papers [38] examined the prospect of such adjustable scales particularly with regard to a possible crossover of viscosities of supercooled liquids from Arrhenius to super-Arrhenius dynamics (see our own analysis for one such glass former

($Zr_{80}Pt_{20}$) in Fig. 2 where the crossover temperature is marked as T_A). We emphasize that it is because the Arrhenius form does not work well (as we illustrated in the previous sections) that we test to see if the functional form of Eq. (18) fits the viscosity data better. Since it includes the Arrhenius form as a special case, Eq. (18) will always allow for a broader collapse of the data than when F is constrained to an Arrhenius form. If the resultant viscosity collapse does not extend over a significant range of scaled temperatures (T/T_{sc}) then the deviation from any attempted scaling of such a form will be even stronger (i.e., no collapse appears even if the function F in Eq. (18) is not restricted to be the exponential function associated with the Arrhenius fit). We determined the values of T_{sc} and η_0 by maximizing the overlap between the $\ln(\eta/\eta_0)$ versus T_{sc}/T curves of the different fluids. Towards this end, we calculated, for any pair of fluids, the discretized integral of the squared difference [a sum of squared errors (SSE)] between scaled viscosity curves of the two fluids. We then found the values of scaling parameters T_{sc} and $\ln \eta_0$ that minimized the resulting latter SSE when the latter was summed over all $N(N-1)/2$ pairs of fluids.

For any two different liquids, there is a specific SSE value. For 38 different liquids, there are 703 pairs of liquids and 703 SSE values. Taking the sum of all 703 SSE values, we obtain an overall SSE, which will vary with the change of each liquid's T_{sc} and η_0 . By adjusting T_{sc} and η_0 for each liquid, we are able to minimize the overall SSE and to optimize our collapsed curve. The values of T_{sc} and η_0 after the adjustment are therefore our optimum T_{sc} and η_0 values.

In Fig. 6, we display our test results for a possible general viscosity collapse of high temperatures liquids with an unconstrained function F in Eq. (18) that is not, necessarily, of an Arrhenius form. As seen therein, the scaled viscosities of several liquids (e.g., $Cu_{50}Zr_{40}Ti_{10}$, OTP, H_2O , etc.) track each other over many decades. The silicate SiO_2 , a quintessential “strong” glass former with relatively small deviations from Arrhenius dynamics upon supercooling to low temperatures, also displays somewhat minute differences from activated dynamics at high temperatures relative to the other liquids that we examined. The viscosity of some fluids may be collapsed in this way onto one another over many decades of the viscosity while for other fluids an attempted collapse yields more fleeting results—a viscosity collapse does not appear for all liquid types in unison. The values of T_{sc} that we found for various fluids are often close to the values of T_A (see Table I) associated with deviations from approximate high temperature Arrhenius dynamics.

In Fig. 7(a), we plot for several liquids, similar to Fig. 5, the numerical proxy ΔS_{slope} for the effective entropy of Eq. (16) as a function of the temperature T . In Fig. 7(b), we provide, similar to Fig. 1, values of (i) the activation energy (left vertical axis in panel (b)) and the viscosity prefactor (right axis) as computed from Eqs. (13) and (14).

IX. A LOWER SCALE BOUND ON THE VISCOSITY

As we briefly reviewed in the Introduction, the viscosity of various compounds is typically minimal at a crossover between their gaseous and fluid phases. Several investigations [29,38,40,41] suggested a lower bound on this viscosity min-

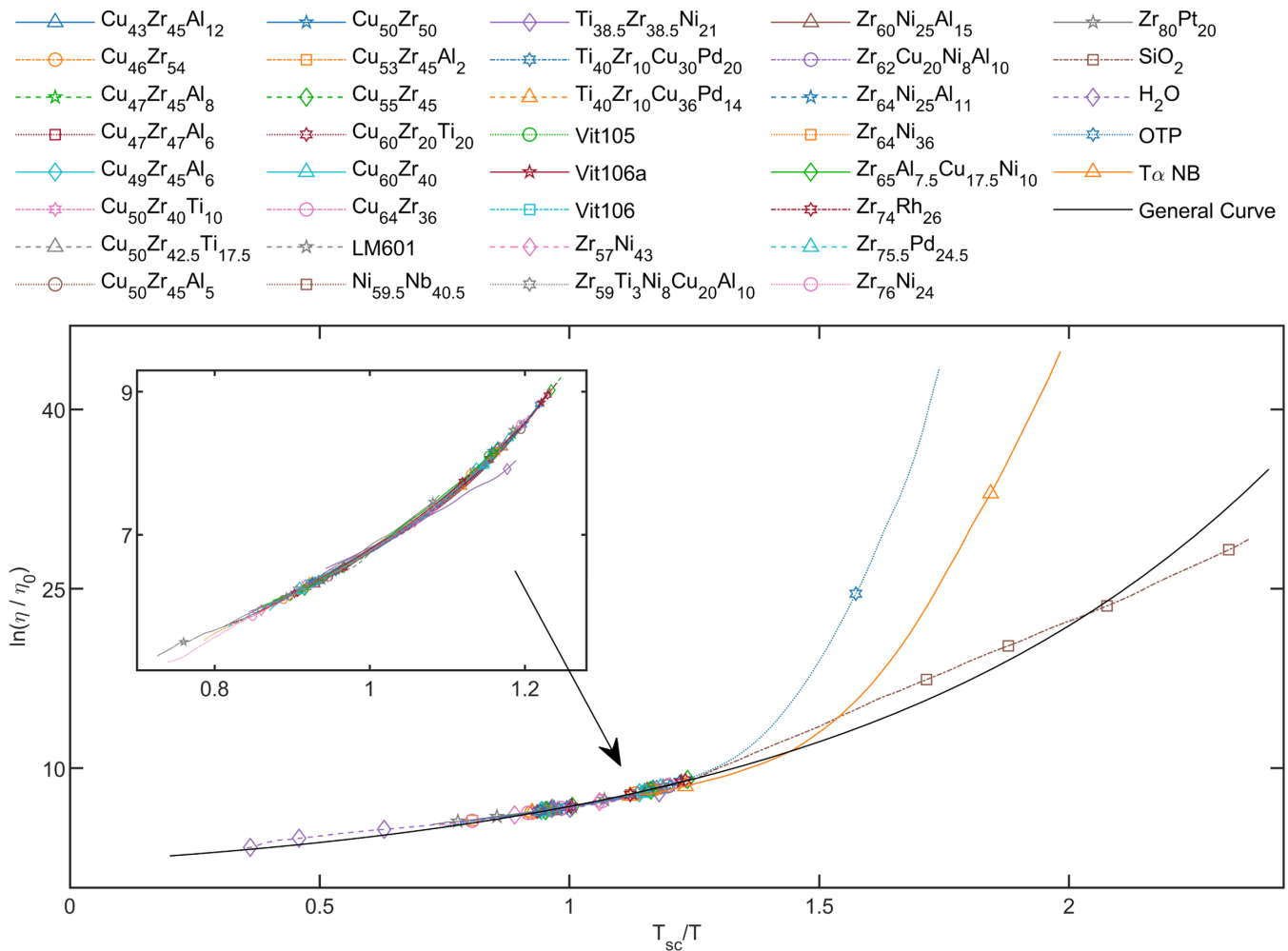


FIG. 6. A test of a possible universal dimensionless collapse of the viscosity of liquids of different types (OTP, H_2O , and numerous metallic liquids). For B_2O_3 , $\text{T}\alpha\text{NB}$, SiO_2 , and OTP, the scaled curves collapse for $T_{sc}/T < 1.25$. The values of T_{sc} and η_0 associated with the displayed viscosity collapse are provided in Table I. The black dashed curve represents the collapse curve $\ln(\eta/\eta_0) = 2.111e^{(1.19(T_{sc}/T))}$.

imum. In this section, we discuss two interrelated bounds and illustrate that they are satisfied for the liquids that we examined. The first bound is that of Eqs. (6) and (15) [29,38,41]. A related second bound, proposed by [40] (TB), can be expressed as

$$\eta \geq \frac{nh}{8\pi^2} \sqrt{\frac{m}{m_e}}. \quad (19)$$

Here, m_e is the electron mass, and m is the mass of the molecules forming the liquid. With $M = (m/(1836m_e))$ denoting the molecular mass of the fluid, the bound of Eq. (6) is lower by a factor of $\sim 0.543\sqrt{M}$ relative to the TB bound of Eq. (19) (dashed-pink line). In Fig. 8, we tested these bounds against available experimental data. For H_2O , the viscosity minimum at 800 K saturates the TB bound. In Fig. 8, we further include, for comparison, two extended Arrhenius type forms (one with the temperature dependent E_{slope} and $\eta_{0,\text{slope}}$ and the other with temperature independent E_{avg} and $\eta_{0,\text{avg}}$) shown in blue and green. Both of these Arrhenius type functions deviate substantially from the measured viscosity curve. These deviations underscore the invalidity of the Arrhenius form for describing the viscosity of these systems. Over the temperature range shown for water, a strong deviation from

Arrhenius is mandated since the viscosity rises with increasing temperature in sufficiently high temperature gases. The other three systems displayed in Fig. 8 ($\text{Zr}_{80}\text{Pt}_{20}$, B_2O_3 , and $\text{Cu}_{50}\text{Zr}_{50}$) are all far below their respective boiling temperatures.

X. CONCLUSIONS

We tested the validity of Arrhenius form for describing the dynamics of general liquids at temperatures above those of melting (and other possible crossovers) by carefully analyzing viscosity data and contrasting it with Eq. (5). We applied an equidistant interpolation of the data and partitioned the temperature range into equal intervals. Subsequently, we applied a low-pass FIR filter to reduce the data noise. We computed the values of the putative uniform activation energy E (and prefactor η_0) of Eq. (5) at 0.25 K temperature intervals.

(i) Our analysis indicates that the viscosity of the liquid (at all temperatures within that phase) is far more complex than a simple Arrhenius behavior with a single temperature independent activation energy E . Perusing Fig. 1 and ensuing analysis, one sees that the viscosity data may be qualitatively captured by the likes of Eq. (2) when, as a general trend the

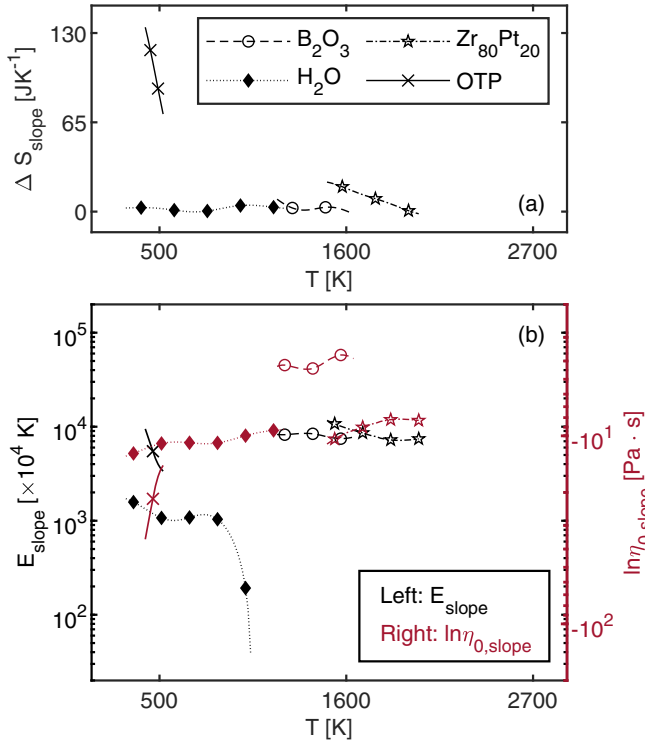


FIG. 7. (a) The effective entropy ΔS_{slope} of Eq. (17) computed with successive temperature differences of size $\Delta T = 15 \text{ K}$ and (b) the activation energy E and the values of η_0 as a function of temperature above T_{sc} for selected liquids except SiO_2 and $\text{T}\alpha\text{NB}$ (see text) above their T_{sc} . For these two liquids, the values of T_{sc} are higher than the examined temperature range and are thus not shown in the figure.

Gibbs free energy activation barrier ΔG typically increases as the temperature T decreases. Equivalently, dispensing with local (in temperature) fluctuations, the associated *effective entropic contribution* $\Delta S = -\frac{\partial \Delta G}{\partial T}$ is generally large and positive. These trends are highlighted in Fig. 5.

(ii) We tested whether activated (more general than Arrhenius) dynamics might still appear universally in high temperature liquids. Towards that end, we examined the extent to which it is possible to collapse dimensionless viscosity data of different fluids as a function of a scaled dimensionless temperature and found that several fluids (of very different composition) exhibit strikingly similar behaviors over many decades of viscosity while others are more divergent. We caution that our results and analysis concern only the viscosity. *We do not exclude possible Arrhenius behaviors of other transport coefficients.*

(iii) We found that the scale of the viscosity of metallic fluids is consistent with that provided by Eq. (15) with n being the particle number density and h Planck's constant. More generally, we find that the lower bound scale of Eq. (6) holds empirically in both the metallic and nonmetallic fluids that we examined.

In the Appendix, we further contrast the empirical viscosity data with several earlier fits in the literature (that were largely introduced for various glass formers). While the most prevalent fits assume a constant Arrhenius form at high

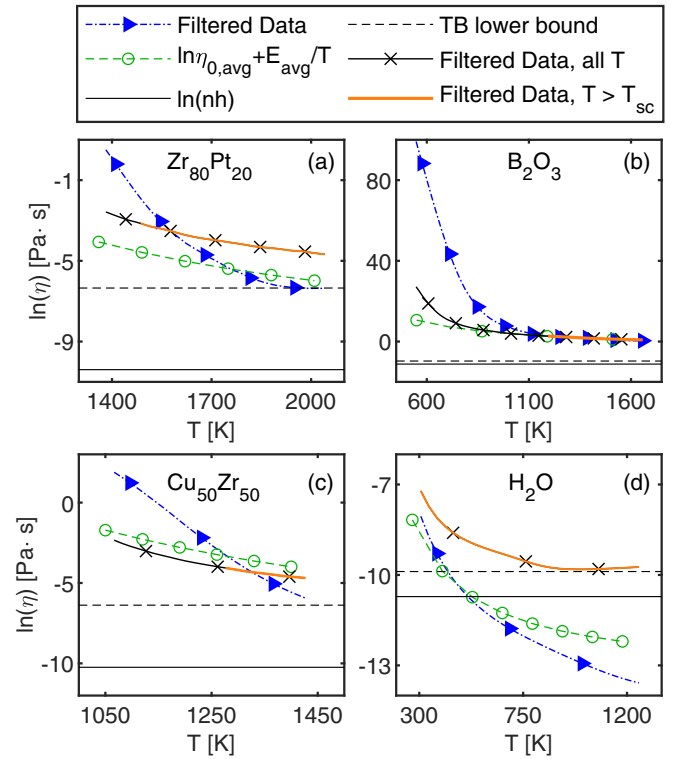


FIG. 8. Comparison of different lower bounds of the viscosity for (a) $\text{Zr}_{80}\text{Pt}_{20}$, (b) B_2O_3 , (c) $\text{Cu}_{50}\text{Zr}_{50}$, and (d) H_2O above their liquidus temperature T_l . The black only portion of the continuous curve is comprised of filtered data points having temperature $T > T_l$ while the overlaid orange portion of that curve provides the viscosity in the temperature range $T > T_{sc}$. In (d), the data range is such that these black and orange data points completely overlap. The bottom solid-horizontal line marks the value of $\ln(nh)$ whose scale is a proposed lower bound of viscosity [29,38,41] and the dashed line is a more recent bound suggested by [40] [Eq. (19)]. The blue curve represents the Arrhenius form with temperature dependent $\eta_{0,\text{slope}}$ and E_{slope} , while the green-dashed curve refers to the Arrhenius form with constant $\eta_{0,\text{avg}}$ and E_{avg} . In these and all other fluids that we investigated, the raw viscosity data was consistent with the two viscosity bounds of Eqs. (6) and (19).

temperatures, some do not. In particular, the MYEGA form [61,62]

$$\ln \eta = \ln \eta_0 + \frac{K'}{T} e^{C/T} \quad (20)$$

(with material dependent parameters η_0 , K' , and C), and the DHTDSJ fit [63]

$$\ln \eta = \ln \eta_0 + \frac{W_0}{k_B T} e^{-T/T_w} \quad (21)$$

(with its fluid dependent parameters η_0 , W_0 , and T_w), may both be expressed as scaling exponentially in E/T with effective energy barriers $E(T)$ that (unlike the Arrhenius form) increase as the temperature T is decreased. The more rapid rise of the viscosity than predicted by activated dynamics dominated by a uniform energy barrier is a feature that we find in all liquids. In accord with these data trends, the MYEGA and DHTDSJ fits that allow (with adjustable additional parameters) for effective activation energies to become larger

as the temperature drops fit the viscosity data better than the Arrhenius form that, as we demonstrated in the current paper, exhibits sizable variations from the experimental data. There are various possible extensions of our extensive analysis of the viscosity of disparate fluids that formed the focus of the current study to disparate response functions- e.g., tests of the Arrhenius and Eyring forms for dielectric relaxation rates. Additionally, the relation between our findings regarding the temperature dependence of the effective activation behavior in equilibrated high temperature liquids and the far more dramatic “super-Arrhenius” viscosity of supercooled liquids [21,22,24,27–34] would be interesting to explore.

We conclude with a more speculative remark. Following recent elegant analysis by Bagioli and Zaccone [64,65], the density of states in the liquid is given by

$$g(\omega) \sim \frac{\omega}{\omega^2 + \Gamma^2} e^{-\omega^2/\omega_D^2}, \quad (22)$$

with ω_D an effective Debye frequency (such that the last factor introduces a soft cutoff) and Γ a temperature dependent damping rate constant. As pointed out by [64], this enables the computation of thermodynamic observables such as, e.g., the specific heat contribution from these instantaneous normal modes [64],

$$c_v = k_B \int_0^\infty d\omega \frac{g(\omega) \frac{\hbar\omega}{2k_B T}}{\sinh^2 \frac{\hbar\omega}{2k_B T}}. \quad (23)$$

Given our findings in the current work of deviations from activated dynamics in general fluids, instead of assuming that Γ obeys an Arrhenius type behavior [64], we may attempt to, more generally, set Γ equal to the reciprocal of the temperature dependent measured relaxation time, i.e., $\Gamma = \tau^{-1}$, with τ determined by the Maxwell relation of Eq. (4). This may fortify [64,65] so as to afford a general link between dynamics (τ) and thermodynamics (c_v) in fluids whose deviation from Arrhenius dynamics is marked over the pertinent temperature range. While such a link seems logical, caution must be paid to the contributions of the different frequencies to the dynamic and thermodynamic properties. The order of magnitude inconsistencies suggest that additional frequency contributions other than those in Eq. (22) may need to be included in $g(\omega)$. Towards this end, we comment on a discrepancy encountered when assuming the single damping rate (and Debye frequency) term of Eq. (22) to capture both the heat capacity and viscosity data at different temperatures. Indeed, the viscosity of liquids may be typically dominated by low frequency hydrodynamic modes whereas the heat capacity can be controlled by far stiffer short range Debye type elastic modes. For instance, for water, the latter hydrodynamic damping rate Γ is 10^{-1} Hertz whereas the scale of the frequency with dominant contributions to the heat capacity is 10^{13} Hertz [66]. We leave the detailed analysis of the above suggested link to a future investigation.

ACKNOWLEDGMENTS

We gratefully acknowledge support by NSF Grant No. DMR 1411229 (Z.N.), which has since been terminated and NSF Grant No. DMR 1904281 (K.F.K.). We further wish to

thank the Aspen Center for Physics (supported by NSF Grant No. PHY-1607611) where some of this work was written.

APPENDIX A: SELF-CONSISTENCY CHECKS

It is illuminating to test the Arrhenius form by reinserting our obtained E and $\ln \eta_0$ into Eq. (8). If the Arrhenius equation is valid then, up to reasonable scatter in the data, the activation energies $E(T)$ (and associated prefactors η_0) will assume constant “average” values E_{avg} (and $\eta_{0,\text{avg}}$). To compute E_{avg} (and $\eta_{0,\text{avg}}$), we take the equal weight uniform average of E_{slope} (and $\eta_{0,\text{slope}}$) over the temperature range, which is from T above T_{sc} to the maximum temperature of our liquids data range.

We may then substitute these average values E_{avg} and $\ln \eta_{0,\text{avg}}$ into Eq. (8) and compare $\ln \eta = \ln \eta_{0,\text{avg}} + E_{\text{avg}}/T$ with the experimental data and contrast the so obtained $\ln \eta_{0,\text{avg}}$ from the experimental data with the theoretical prediction of Eq. (15). In Fig. 3(a), an Arrhenius fit with E_{avg} and $\ln \eta_{0,\text{avg}}$ (marked in red) is consistent with the raw data (the black curve in this figure) only at temperatures close to $T_{sc} = 1482\text{K}$. The Arrhenius curve and the actual raw experimental data substantially deviate from one another when extrapolating to higher (and lower) temperatures. We next tested how an agreement with the Arrhenius form might be ameliorated if we compute the average values E_{avg} and $\ln \eta_{0,\text{avg}}$ over a narrower temperature range. Towards this end, we calculated the above E_{avg} and $\ln \eta_{0,\text{avg}}$ by averaging over the temperature interval between T_{A^*} to T_{max} (where $T_{A^*} > T_{sc}$). Here, T_{max} denotes the highest temperature for which experimental data are available. Evaluating these averages, we found that the data and Arrhenius form with the above values matched in a limited range near T_{A^*} . As we progressively shortened the temperature range over which the averages were taken (by fixing T_{max} and raising T_{A^*}), the Arrhenius (red) curve in Fig. 3(a) continued to deviate from the experimental data at gradually higher temperature.

We further explored the consistency of Eq. (15) with the experimental data, where $E_{\text{avg}} = 8225\text{K}$ and $\ln(nh) = -10.394\text{Pa} \cdot \text{s}$ for $\text{Zr}_{80}\text{Pt}_{20}$. As Fig. 3(a) underscores, an order of magnitude disparity may appear between Eq. (15) and the experimental data—the scale of η_0 associated with the fitted measured viscosity of $\text{Zr}_{80}\text{Pt}_{20}$ is, approximately, $e^{1.6} \sim 5$ times larger than the product nh . As seen in Fig. 3(b), for H_2O the corresponding ratio between η_0 and (nh) is far larger, being approximately $e^6 \sim 400$. Due to measurement errors and the form of the raw experimental data, the temperature intervals may not, generally, be judiciously chosen so as to be of uniform width. Consequently, we cannot collate all of the calculated slopes into one figure to see how they vary with the temperature since each slope has different denominator values when employing Eqs. (13) and (14).

APPENDIX B: RELIABILITY OF RESULTS

We need to assess whether our obtained effective $E(T)$ and $\eta_0(T)$ are reliable. Addressing this question requires us to find the extent to which the FIR filter may impact the determined $E(T)$ and $\eta_0(T)$. The defining property of our (and any) FIR

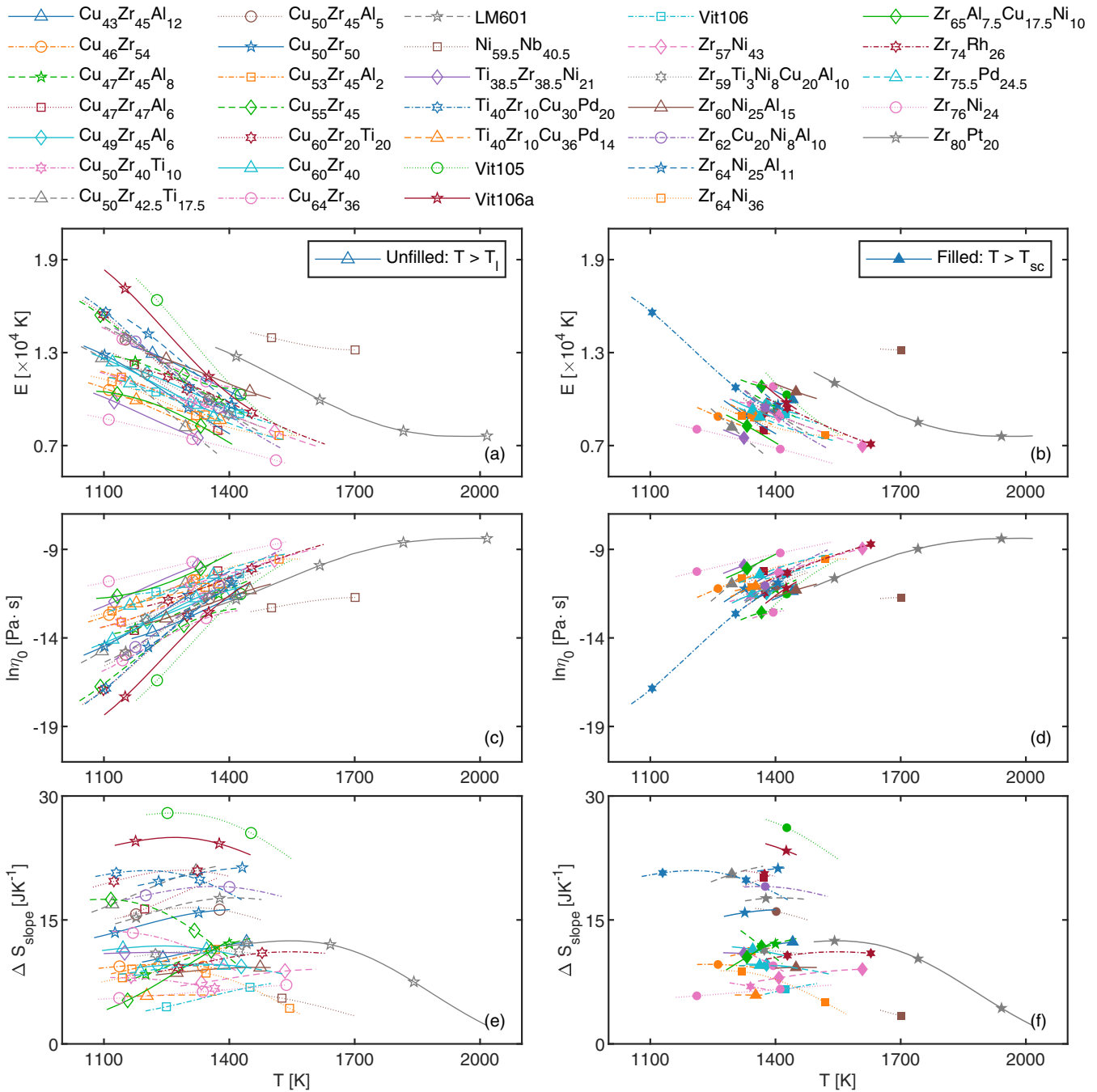


FIG. 9. Activation energy E [Eq. (9)], viscosity prefactor η_0 [Eq. (10)], and effective entropy ΔS_{slope} of Eq. (17) as a function of temperature of various fluids above their liquidus temperature T_l (unfilled markers) and their scaling temperature T_{sc} (filled markers).

filter is the absence of feedback in its application generally endowing it with an intrinsic stability.

In the main text, we reported on our tests of the validity of Arrhenius form by plotting both the activation energy $E(T)$ and the prefactor $\eta_0(T)$ as functions of temperature. Trends in $E(T)$ and $\eta_0(T)$ become clearer when these are smooth and monotonous. However, if we apply the finite difference equations of Eq. (13) or Eq. (14) directly to the raw viscosity data, then $E(T)$ or $\eta_0(T)$ will, generally, exhibit large fluctuations. These fluctuations can obscure trends in either the activation energy E or the viscosity prefactor $\eta_0(T)$.

Ideally, reducing the width of the temperature interval in Eq. (13) and Eq. (14) may, in principle, allow for a more accurate determination of an effective activation energy $E(T)$ or the viscosity prefactor $\eta_0(T)$. However, the use of smaller intervals will, inevitably, enhance any noise present in the data. Due to the measurement errors and the detailed form of the raw experimental data, generally, the temperature intervals may not chosen to identically be equal. To deal with the problem of varying width temperature intervals, we applied equidistant interpolation. To mitigate the inherent noise in

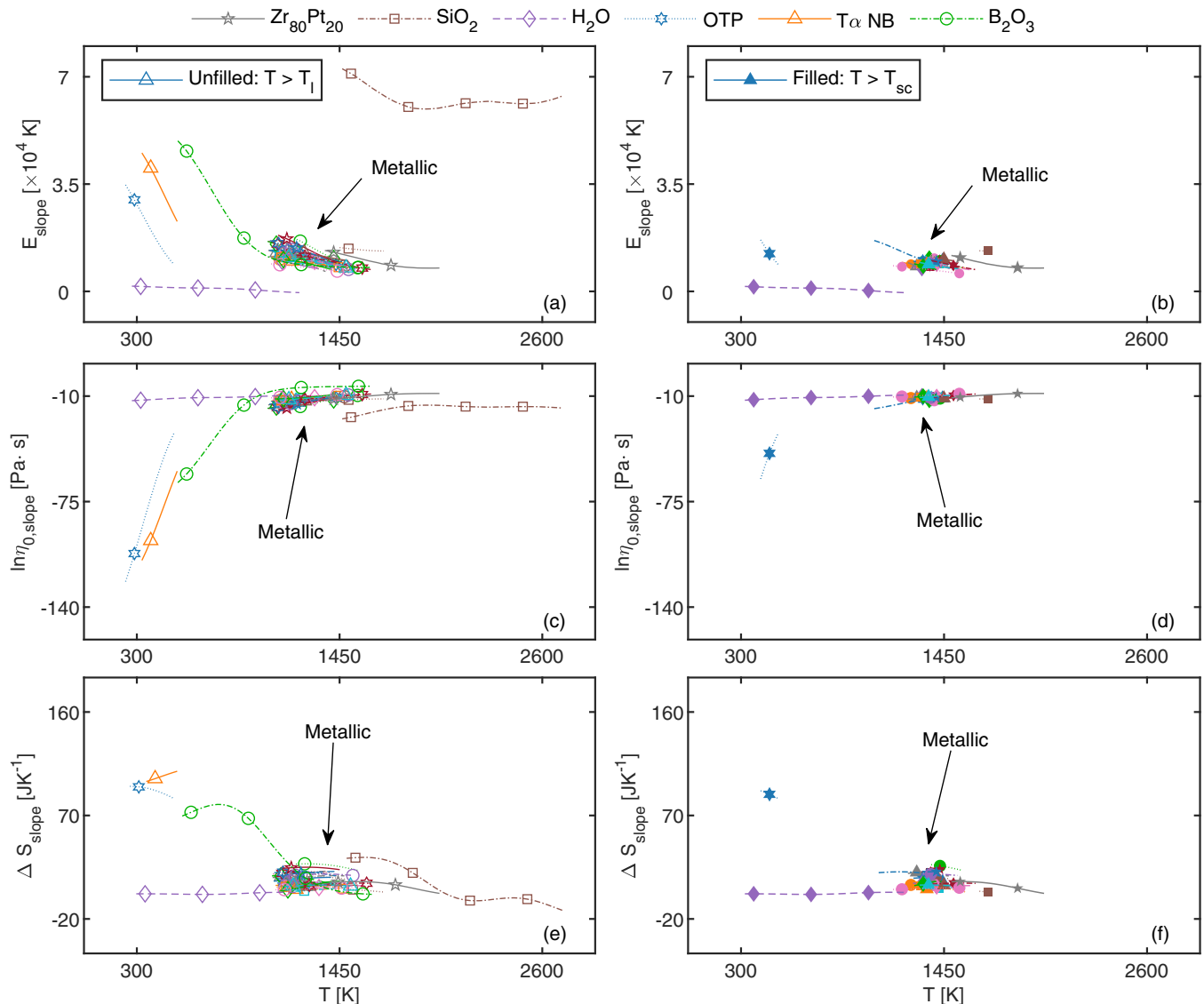


FIG. 10. Similar to Fig. 9, we plot the activation energy E [Eq. (9)], viscosity prefactor η_0 [Eq. (10)], and the effective entropy ΔS_{slope} of Eq. (17) as a function of temperature of several liquids above their liquidus temperature T_l (unfilled markers) and their scaling temperature T_{sc} (filled markers). Related results are shown in Fig. 7 and Fig. 9. Here, we provide data for additional fluids. For SiO_2 and $\text{T}\alpha\text{NB}$ (see text), the values of the scaling temperature T_{sc} are higher than the examined temperature range and are therefore not shown in the figure.

the data, we designed and applied a low-pass FIR filter with equidistant interpolation.

We applied the FIR filter to the raw viscosity data $\eta(T)$ instead of the extracted $E(T)$ or $\eta_0(T)$. This was done since $E(T)$ and $\eta_0(T)$ are approximate measures derived from the raw data. In Fig. 1, we provided extracted finite difference numerical values of $E(T)$ and $\eta_0(T)$ for six selected liquids above their liquidus temperature T_l . In this Appendix, we separately plot $E(T)$ and $\eta_0(T)$ of all tested metallic liquids above their liquidus temperature T_l and scaling temperature T_{sc} in Figs. 9 and 10.

In Table II, we provide statistics regarding the quality of our fits. These figures of merit, computed for both the raw and filtered data, are comprised of R-square (R^2) values and the sum of squared errors (SSE).

APPENDIX C: FURTHER COMMENTS ON ESTIMATING E AND η_0 VALUES FROM FITS

As discussed in the main text, Eq. (8) enables the extraction of the effective E and $\ln \eta_0$ at different temperatures. Our filtered data were chosen to be equally spaced allowing us to fit adjacent data points with Eq. (8). For example, for the temperature domain $[T_i, T_{i+1}]$ and the corresponding range of viscosity $[\ln \eta_i, \ln \eta_{i+1}]$, the fitting outputs will be E_i and $\ln \eta_{0,i}$ at the temperature $T_{i+1/2}$. Similarly, for the temperature interval $[T_{i+1}, T_{i+1+1}]$, the outputs are E_{i+1} and $\ln \eta_{0,i+1}$ at $T_{i+1+1/2}$, etc.

Our initial analysis centered on temperature intervals of width $\Delta T = T_{i+1} - T_i = 0.25 \text{ K}$. Such relatively small temperature intervals ΔT increase the uncertainties in E and $\ln \eta_0$ and introduce oscillations in $E(T)$ and $\ln \eta_0(T)$. To avoid

TABLE II. Statistical residuals of fitting results. The first four columns are the residuals when fitting the raw and filtered data with Arrhenius form Eq. (10) with the whole data range, and the 4th and 5th columns are the R^2 results when fitting $T < T_A$ and $T > T_A$ with myrefeq:200. The uncertainty of each liquid comes from the liquids' density's liquids. The uncertainty of E is determined by evaluating the maximum amplitude of the oscillated curve.

Composition	SSE (raw) [10^{-5}]	R^2 (raw) (All T)	SSE (filter) [10^{-5}]	R^2 (filter) (All T)	R^2 (filter) ($T < T_A$)	R^2 (filter) ($T > T_A$)	Uncertainty of E [$\times 10^4$ K]
Cu ₄₃ Zr ₄₅ Al ₁₂	1.576	0.9502	3.863	0.9998			0.2
Cu ₄₆ Zr ₅₄	8.125	0.9489	2.123	0.9982			0.25
Cu ₄₇ Zr ₄₅ Al ₈	4.016	0.9339	1.908	0.9943			0.3
Cu ₄₇ Zr ₄₇ Al ₆	5.112	0.894	2.214	0.9857			0.2
Cu ₄₉ Zr ₄₅ Al ₆	1.237	0.9735	5.121	0.9987			0.25
Cu ₅₀ Zr ₄₀ Ti ₁₀	4.522	0.9032	0.936	0.9972			0.2
Cu ₅₀ Zr _{42.5} Ti _{7.5}	1.518	0.9874	6.006	0.9947			0.25
Cu ₅₀ Zr ₄₅ Al ₅	1.512	0.9727	3.214	0.9936	0.9912	0.9918	0.2
Cu ₅₀ Zr ₅₀	3.231	0.9281	2.489	0.9951	0.9941	0.9948	0.3
Cu ₅₃ Zr ₄₅ Al ₂	3.667	0.9465	1.844	0.9972			0.3
Cu ₅₅ Zr ₄₅	3.941	0.9016	2.841	0.9906			0.2
Cu ₆₀ Zr ₂₀ Ti ₂₀	1.254	0.9612	0.609	0.9955	0.9836	0.9964	0.2
Cu ₆₀ Zr ₄₀	5.126	0.9189	4.263	0.9966			0.2
Cu ₆₄ Zr ₃₆	3.12	0.8317	2.607	0.9834			0.2
LM601	1.039	0.9665	11.03	0.9883			0.2
Ni _{59.5} Zr ₃₆	1.924	0.9699	9.659	0.9756			0.2
Ti _{38.5} Zr ₃₈ Ni ₂₁	4.199	0.9839	5.615	0.9969			0.2
Ti ₄₀ Zr ₁₀ Cu ₃₀ Pd ₂₀	2.653	0.9496	0.652	0.9986			0.25
Ti ₄₀ Zr ₁₀ Cu ₃₆ Pd ₁₄	3.162	0.9513	0.7	0.9977	0.9995	0.9951	0.3
Vit105	4.566	0.9732	2.049	0.9983			0.2
Vit106	0.001098	0.9873	0.00274	0.9951	0.9982	0.9996	0.2
Vit106a	2.585	0.9546	1.623	0.9962	0.9886	0.9965	0.2
Zr ₅₇ Ni ₄₃	18.89	0.976	5.535	0.998			0.2
Zr ₅₉ Ti ₃ Ni ₈ Cu ₂₀ Al ₁₀	2.797	0.9585	1.694	0.9977			0.2
Zr ₆₀ Ni ₂₅ Al ₁₅	1.201	0.9847	1.896	0.9969			0.2
Zr ₆₂ Cu ₂₀ Ni ₈ Al ₁₀	2.34	0.9866	1.563	0.9928			0.2
Zr ₆₄ Ni ₂₅ Al ₁₁	6.04	0.8718	0.908	0.998			0.3
Zr ₆₄ Ni ₃₆	4.211	0.9015	1.788	0.9972	0.9966	0.9985	0.3
Zr ₆₅ Al _{7.5} Cu _{17.5} Ni ₁₀	12.01	0.9551	15.42	0.9915			0.2
Zr ₇₄ Rh ₂₆	232.4	0.9866	564	0.9929			0.15
Zr _{75.5} Pd _{24.5}	232.4	0.9843	998.2	0.991			0.2
Zr ₇₆ Ni ₂₄	19.13	0.9919	195.7	0.9983	0.9999	0.9994	0.2
Zr ₈₀ Pt ₂₀	2.001	0.9913	0.997	0.9984	0.997	0.9935	0.35
H ₂ O	17.5	0.9233	2.45	0.9932			0.2
B ₂ O ₃	4.017	0.9542	1.066	0.9961			0.1
OTP	3.018	0.9332	1.656	0.9947			0.3
T α NB	2.89	0.9611	1.788	0.9936			0.2
SiO ₂	1.526	0.9991	0.956	0.9977			0.1

these spurious effects and generate more monotonous trends, we varied the width of the temperature intervals over which we compute the averages. As this latter width increases, the resulting $E(T)$ and $\ln \eta_0(T)$ curves become smoother as more fluctuations are removed. When this factor is large enough, the general monotonic trends of E and $\ln \eta_0$ become lucid. For instance, if this scaling factor is 60 then the temperature intervals will be $[T_{60i}, T_{60(i+1)}]$.

Figure 4 shows, respectively, the values of $E(T)$ and $\ln \eta_0(T)$ for Zr₈₀Pt₂₀ that were obtained in this way. The temperature window scaling factor is 60 with a corresponding the temperature interval width $\Delta T = 15$ K. As the temperature rises from 1400 K to 1900 K, the effective activation energy E drops from 11 000 K to 6000 K whereas $\ln \eta_0$

increases from -10.7 to -9 . As we noted earlier, from Eq. (12) [a trivial restatement of Eq. (8)], when $T \ln \eta$ is examined as a function of the temperature, the activation energy E becomes the intercept and $\ln \eta_0$ is the slope.

APPENDIX D: ADDITIONAL VISCOSITY FITS

Aside from the MYEGA [61] and DHTDSJ [63] fits of Eqs. (20) and (21) (the inception of which was motivated by the behavior of glass formers), there are numerous other fitting forms that attempt to describe the viscosity of fluids at high temperatures (as well as the viscosities of bona fide super-

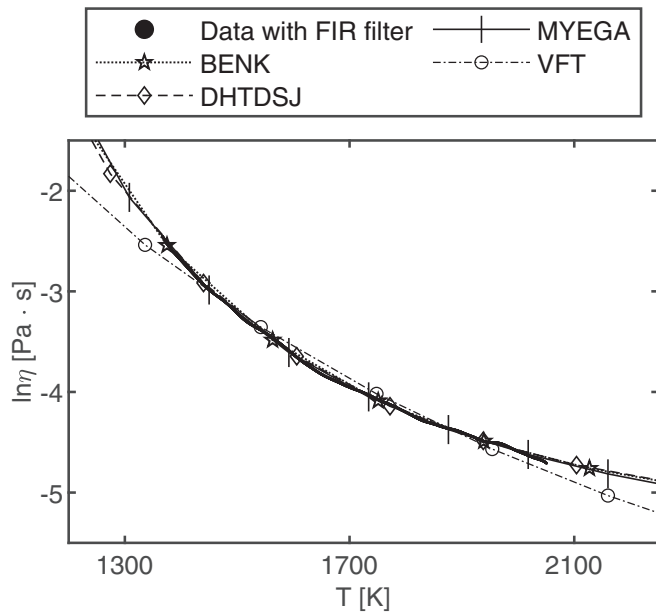


FIG. 11. A comparison between our experimentally measured filtered viscosity data of $Zr_{80}Pt_{20}$ with four fitting forms: BENK [Eq. (D4)], DHTDSJ [Eq. (21)], MYEGA [Eq. (20)], and VFT [Eq. (D1)].

cooled liquids at temperatures below equilibrium freezing). For concreteness, we list several of these below.

We start by noting perhaps by the far most common empirical form, that of Vogel, Fulcher, and Tammann (VFT) [67–69]. Herein,

$$\ln \eta(T) = \ln \eta_0 + \frac{B}{T - T_A} \quad (D1)$$

with material dependent parameters η_0 , B , and T_A .

According to the KKZNT [42–44] fit for the viscosity

$$\ln \eta(T) = \ln \eta_0 + \frac{E_\infty}{T} + \frac{T_A}{T} B \left(\frac{T_A - T}{T_A} \right)^z \Theta(T_A - T), \quad (D2)$$

where η_0 , E_∞ , T_A , and z are liquid dependent adjustable constants (with, in most fluids, $z \simeq 8/3$).

The DEH [45] fit asserts that

$$\ln \eta(T) = \ln \eta_0 + \frac{E_\infty}{k_B T} + \frac{(T - T_A)^2}{2a^2} \Theta(T_A - T), \quad (D3)$$

with η_0 , E_∞ , a , and T_A being material dependent parameters.

Another functional form (BENK) [38] that we studied suggests that

$$\ln \eta(T) = \ln \eta_0 + \frac{E}{k_B T} + J^2 \left(\frac{1}{T} - \frac{1}{\tilde{T}} \right)^2 \Theta(T_A - T). \quad (D4)$$

Here, the adjustable, fluid dependent, constants are η_0 , J , \tilde{T} , and T_A .

Numerous functional forms and theoretical approaches including, in particular those related to the enigmatic glass transition, appear in the literature, e.g., [21–24,27–34]. Some of these, similar to the above forms build on Arrhenius type notions and various modifications of this form. An Arrhenius

type analysis was recently pursued in [70],

$$\ln \eta(T) = \ln \eta_0 - \frac{b}{k_B} + \frac{Q_a^*}{k_B T}. \quad (D5)$$

Here, Q_a^* is the effective activation energy computed by Eq. (9). When computed from viscosity data of supercooled liquids, this effective energy barrier exhibits a peak around the glass transition T_g . This led [70] to posit that the glass transition is associated with a bona fide phase transition at T_g . In Fig. 11, we compare several fitting functions for the viscosity over a temperature interval that includes the liquidus temperature ($T_l = 1450$ K) of $Zr_{80}Pt_{20}$.

In Eqs. (D1)–(D4), T_A (see also a brief discussion in the main text) denotes a crossover temperature from a putative Arrhenius behavior ($T > T_A$) to super-Arrhenius scaling ($T < T_A$). Equation (D5) does not invoke a crossover temperature.

Our results concerning the high temperature deviations from activated dynamics (including temperatures above assumed crossover temperatures) suggest that the VFT, KKZNT, DEH, and BENK fits and similar others that assume high temperature Arrhenius dynamics do not accurately describe

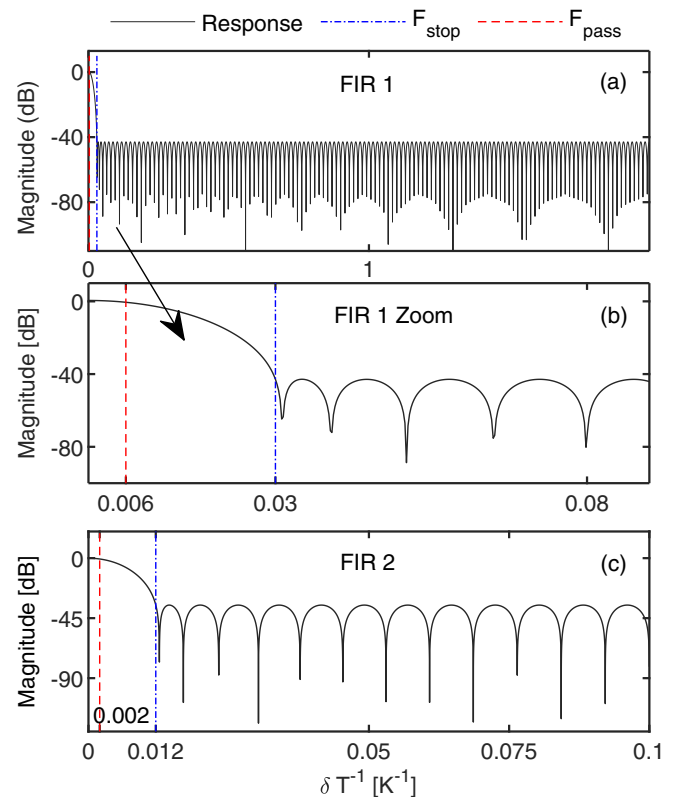


FIG. 12. The amplitude response of two low-pass FIR filters (labeled FIR 1 and FIR 2). The abscissa denotes the number of samples per inverse temperature interval $1/\delta T$. The ordinate marks the magnitude of attenuation of the filter. The red- and blue-dashed lines indicate, respectively, the sample rate at F_{pass} and F_{stop} . As all panels of this figure illustrates, the (black) response curve starts to oscillate for sample rates beyond F_{stop} . Panel (b) is a blow up of FIR 1's amplitude response (Panel a). Here, $F_{\text{pass}} = 0.006$ K^{-1} and $F_{\text{stop}} = 0.03$ K^{-1} . In Panel (c), we provide a blow up of FIR 2's response with $F_{\text{pass}} = 0.002$ K^{-1} and $F_{\text{stop}} = 0.012$ K^{-1} .

TABLE III. The low-pass FIR filters that we used to filter the viscosity data. FIR1 filters the raw viscosity data with $\Delta T = 0.25$ K. For FIR2, $\Delta T = 5$ K, and 15 K. Both FIR1 and FIR2 are generated by the software MATLAB.

Filter	FIR1	FIR2
Specify Order	260	25
F_s	4 K^{-1}	0.067 K^{-1}
F_{pass}	0.006 K^{-1}	0.002 K^{-1}
F_{stop}	0.03 K^{-1}	0.012 K^{-1}

high temperature liquids. Our finding does not exclude the asserted functional forms of these fits at all temperatures—only their behaviors at high temperatures. By contrast, fits like those of Eqs. (20) and (21) that, at all T (in particular, also for all temperatures above equilibrium melting), exhibit an effective activation barrier $E(T)$ that monotonically decreases with increasing temperature are consistent with the trends that we universally find in all examined high temperature fluids.

APPENDIX E: LOW-PASS FILTER

In the current paper, we invoked ideas similar to those used in standard frequency filters and (given that our viscosity data are a function of temperature and not time) extended these to the temperature domain (i.e., with $\frac{1}{\Delta T}$ playing the role of frequency in the typically used filters [71]). Figure 12 and Table III provide basic schematics of our low-pass FIR filter (FIR1) for the viscosity data, while Figs. 12 provide the schematics of our second FIR filter for determining the

activation energy and effective entropy. When applying an equidistant interpolation to our viscosity data, the temperature interval between each two adjacent data points is $\Delta T = 0.25$ K. Thus, the sampling rate of the filter is $F_s = 1/\Delta T = 1/0.25 \text{ K} = 4 \text{ K}^{-1}$. We then increased the width of the temperature windows over which we compute the averages and fitted the decimated data with Eq. (9) to obtain E_{slope} and applied our second FIR filter (FIR 2). Herein, $\Delta T = 15$ K, and the sampling rate of the second filter is $F_s = 1/\Delta T = 1/15 \text{ K} = 0.067 \text{ K}^{-1}$. We repeated this procedure for S_{slope} with our second FIR filter.

Figures 12 illustrate the effects of the two filters. In these figures, the abscissa is the temperature frequency $F_t = 1/\delta T$ (where δT is a temperature interval not smaller than ΔT). The vertical axis is the attenuation magnitude of the filter. The minimal temperature interval used was of width $\Delta T = 0.25$ K (for FIR1) and $\Delta T = 15$ K for (FIR2) and $F_{t,\text{max}} = F_s$.

Whenever F_t is smaller than $F_{\text{pass}} = 0.006 \text{ K}^{-1}$ (FIR1) and 0.002 K^{-1} (for FIR2), filtering leads to no change. By contrast, when $F_{\text{pass}} < F_t < F_{\text{stop}} = 0.03 \text{ K}^{-1}$ (for FIR1) and 0.012 K^{-1} (for FIR2), as F_t increases, the magnitude of the filtered data monotonically decreases (with the filtered data being reduced by 42.9 dB for FIR1 (and 35.2 dB for FIR 2) just above F_{stop} . For $F_t \geq F_{\text{stop}}$, the magnitude of the filtered data remains, approximately, constant. The filter attenuates data sufficiently close to T_i while leaving data far from T_i essentially unchanged. Applying a low-pass FIR filter to the data leads to a smoother and more monotonous result while, concomitantly, preserving the original trends present in the data.

- [1] S. Arrhenius, Über die dissociationswärme und den einfluss der temperatur auf den dissociationsgrad der elektrolyte, *Z. Phys. Chem.* **4U**, 96 (1889).
- [2] S. Arrhenius, Über die Reaktionsgeschwindigkeit bei der inversion von Rohrzucker durch Säuren, *Z. Phys. Chem.* **4U**, 226 (1889).
- [3] K. J. Laidler, The development of the Arrhenius equation, *J. Chem. Educ.* **61**, 494 (1984).
- [4] P. G. Debenedetti and F. H. Stillinger, Supercooled liquids and the glass transition, *Nature (London)* **410**, 259 (2001).
- [5] M. Petrowsky, A. M. Fleshman, and R. Frech, Application of the compensated Arrhenius formalism to fluidity data of polar organic liquids, *J. Phys. Chem. B* **117**, 2971 (2013).
- [6] P. Hänggi, P. Talkner, and M. Borkovec, Reaction-rate theory: Fifty years after Kramers, *Rev. Mod. Phys.* **62**, 251 (1990).
- [7] E. Pollak and P. Talkner, Reaction rate theory: What it was, where is it today, and where is it going? *Chaos* **15**, 026116 (2005).
- [8] H. Eyring, The activated complex in chemical reactions, *J. Chem. Phys.* **3**, 107 (1935).
- [9] G. Adam and J. H. Gibbs, On the temperature dependence of cooperative relaxation properties in glass forming liquids, *J. Chem. Phys.* **43**, 139 (1965).
- [10] N. W. Ashcroft and N. D. Mermin, *Solid State Physics* (Holt, Rinehart, and Winston, New York, 1976)
- [11] D. Samantaray, S. Mandal, and A. K. Bhaduri, A comparative study on Johnson Cook, modified Zerilli-Armstrong and Arrhenius-type constitutive models to predict elevated temperature flow behaviour in modified 9Cr-1Mo steel, *Comput. Mater. Sci.* **47**, 568 (2009).
- [12] R. O. Simmons and R. W. Balluffi, Measurements of equilibrium vacancy concentrations in aluminum, *Phys. Rev.* **117**, 52 (1960).
- [13] Th. Hehenkamp, Absolute vacancy concentrations in noble metals and some of their alloys, *J. Phys. Chem. Solids* **55**, 907 (1994).
- [14] A. Glensk, B. Grabowski, T. Hickel, and J. Neugebauer, Breakdown of the Arrhenius Law in Describing Vacancy Formation Energies: The Importance of Local Anharmonicity Revealed by *Ab Initio* Thermodynamics, *Phys. Rev. X* **4**, 011018 (2014).
- [15] R. J. Cava, R. M. Fleming, P. Littlewood, E. A. Rietman, L. F. Schneemeyer, and R. G. Dunn, Dielectric response of the charge-density wave in $\text{K}_{0.3}\text{MoO}_3$, *Phys. Rev. B* **30**, 3228 (1984).
- [16] A. P. Dioguardi, M. M. Lawson, B. T. Bush, J. Crocker, K. R. Shirer, D. M. Nisson, T. Kissikov, S. Ran, S. L. Bud'ko, P. C. Canfield, S. Yuan, P. L. Kuhns, A. P. Reyes, H.-J. Grafe, and N. J. Curro, Nmr evidence for inhomogeneous glassy behavior driven by nematic fluctuations in iron arsenide superconductors, *Phys. Rev. B* **92**, 165116 (2015).

- [17] I. R. Kleckner and M. P. Foster, An introduction to NMR-based approaches for measuring protein dynamics, *Biochim. Biophys. Acta* **1814**, 942 (2011).
- [18] F. Mallamace, C. Corsaro, D. Mallamace, S. Vasi, and H. E. Stanley, NMR spectroscopy study of local correlations in water, *J. Chem. Phys.* **145**, 214503 (2016).
- [19] J. P. Sutter, S. Tsutsui, R. Higashinaka, Y. Maeno, O. Leupold, and A. Q. R. Baron, Relaxation in the spin ice $\text{Dy}_2\text{Ti}_2\text{O}_7$ studied using nuclear forward scattering, *Phys. Rev. B* **75**, 140402 (2007).
- [20] S. S. Schoenholz, E. D. Cubuk, D. M. Sussman, E. Kaxiras, and A. J. Liu, A structural approach to relaxation in glassy liquids, *Nat. Phys.* **12**, 469 (2016).
- [21] J. S. Langer, Theories of glass formation and the glass transition, *Rep. Prog. Phys.* **77**, 042501 (2014).
- [22] M. D. Ediger, C. A. Angell, and S. R. Nagel, Supercooled liquids and glasses, *J. Phys. Chem.* **100**, 13200 (1996).
- [23] Z. Nussinov, A one parameter fit for glassy dynamics as a quantum corollary of the liquid to solid transition, *Philos. Mag.* **97**, 1509 (2017).
- [24] N. B. Weingartner, C. Pueblo, F. S. Nogueira, K. F. Kelton, and Z. Nussinov, A phase space approach to supercooled liquids and a universal collapse of their viscosity, *Front. Mater.* **3**, 50 (2016).
- [25] Z. Nussinov, Macroscopic length correlations in non-equilibrium systems and their possible realizations, *Nucl. Phys. B* **953**, 114948 (2020).
- [26] Z. Nussinov, N. B. Weingartner, and F. S. Nogueira, The ‘glass transition’ as a topological defect driven transition in a distribution of crystals and a prediction of a universal viscosity collapse, in *Topological Phase Transitions and New Developments* (World Scientific, Singapore, 2018)pp. 61–79.
- [27] C. A. Angell, Formation of glasses from liquids and biopolymers, *Science* **267**, 1924 (1995).
- [28] C. A. Angell, K. L. Ngai, G. B. McKenna, P. F. McMillan, and S. W. Martin, Relaxation in glassforming liquids and amorphous solids, *J. Appl. Phys.* **88**, 3113 (2000).
- [29] Z. Nussinov, F. Nogueira, M. Blodgett, and K. F. Kelton, Thermalization and possible quantum relaxation times in “classical” fluids: theory and experiment, [arXiv:1409.1915](https://arxiv.org/abs/1409.1915).
- [30] K. F. Kelton, Kinetic and structural fragility—A correlation between structures and dynamics in metallic liquids and glasses, *J. Phys.: Condens. Matter* **29**, 023002 (2017).
- [31] A. Jaiswal, T. Egami, K. F. Kelton, K. S. Schweizer, and Y. Zhang, Correlation between Fragility and the Arrhenius Crossover Phenomenon in Metallic, Molecular, and Network Liquids, *Phys. Rev. Lett.* **117**, 205701 (2016).
- [32] H. G. E. Hentschel, S. Karmakar, I. Procaccia, and J. Zylberg, Relaxation mechanisms in glassy dynamics: The Arrhenius and fragile regimes, [arXiv:1202.1127](https://arxiv.org/abs/1202.1127).
- [33] L. Berthier, G. Biroli, J.-P. Bouchaud, L. Cipelletti, and W. van Saarloos, *Dynamical Heterogeneities in Glasses, Colloids, and Granular Media*, Vol. 150 (Oxford University Press, Oxford, 2011).
- [34] L. Berthier and G. Biroli, Theoretical perspective on the glass transition and amorphous materials, *Rev. Mod. Phys.* **83**, 587 (2011).
- [35] O. Reynolds, On the theory of lubrication and its application to Mr. Beauchamp tower’s experiments, including an experimental determination of the viscosity of olive oil, *Philos. Trans. R. Soc. London Ser. I* **177**, 157 (1886).
- [36] J. De Guzman, Relation between fluidity and heat of fusion, *Anales Soc. Espan. Fis. Y. Quim* **11**, 353 (1913).
- [37] E. N. DA C. Andrade, The viscosity of liquids, *Nature (London)* **125**, 309 (1930).
- [38] M. E. Blodgett, T. Egami, Z. Nussinov, and K. F. Kelton, Proposal for universality in the viscosity of metallic liquids, *Sci. Rep.* **5**, 13837 (2015).
- [39] R. J. Greet and D. Turnbull, Glass transition in *o*-terphenyl, *J. Chem. Phys.* **46**, 1243 (1967).
- [40] K. Trachenko and V. V. Brazhkin, Minimal quantum viscosity from fundamental physical constants, *Sci. Adv.* **6**, eaba3747 (2020).
- [41] Z. Nussinov and S. Chakrabarty, Exact universal chaos, speed limit, acceleration, Planckian transport coefficient, “collapse” to equilibrium, and other bounds in thermal quantum systems, *Ann. Phys.* **443**, 168970 (2022).
- [42] D. Kivelson, S. A. Kivelson, X. Zhao, Z. Nussinov, and G. Tarjus, A thermodynamic theory of supercooled liquids, *Physica A* **219**, 27 (1995).
- [43] G. Tarjus, S. A. Kivelson, Z. Nussinov, and P. Viot, The frustration-based approach of supercooled liquids and the glass transition: A review and critical assessment, *J. Phys.: Condens. Matter* **17**, R1143 (2005).
- [44] Z. Nussinov, Avoided phase transitions and glassy dynamics in geometrically frustrated systems and non-Abelian theories, *Phys. Rev. B* **69**, 014208 (2004).
- [45] N. B. Weingartner, C. Pueblo, K. F. Kelton, and Z. Nussinov, Critical assessment of the equilibrium melting-based, energy distribution theory of supercooled liquids and application to jammed systems, [arXiv:1512.04565](https://arxiv.org/abs/1512.04565).
- [46] C. J. Seeton, Viscosity-temperature correlation for liquids, in *International Joint Tribology Conference, Part A: Tribomaterials; Lubricants and Additives; Elastohydrodynamic Lubrication; Hydrodynamic Lubrication and Fluid Film Bearings; Rolling Element Bearings; Engine Tribology; Machine Components Tribology; Contact Mechanics*, (American Physical society of Mechanical Engineers, 2008), Paper No. IJTC2006-12139, pp. 131–142.
- [47] K. Vollmayr-Lee, C. H. Gorman, and H. E. Castillo, Universal scaling in the aging of the strong glass former SiO_2 , *J. Chem. Phys.* **144**, 234510 (2016).
- [48] T. Iwashita, D. M. Nicholson, and T. Egami, Elementary Excitations and Crossover Phenomenon in Liquids, *Phys. Rev. Lett.* **110**, 205504 (2013).
- [49] As we will detail in Sec. VIII (and Fig. 6 therein), a scaling of the temperature by a liquid dependent T_{sc} allows for a collapse [Eq. (18)] of the viscosity data over a broader range of temperatures than simple Arrhenius dynamics. This is so since the function F in Eq. (18) may differ from the simple exponential of Eq. (5).
- [50] W. C. Wilfried, https://commons.wikimedia.org/wiki/File:Dynamic_Viscosity_of_Water.png.
- [51] User:Ojovan, https://upload.wikimedia.org/wikipedia/commons/c/cb/B2O3_viscosoty.jpg.
- [52] D. J. Plazek, C. A. Bero, and I.-C. Chay, The recoverable compliance of amorphous materials, *J. Non-Cryst. Solids* **172-174**, 181 (1994).

- [53] R. H. Doremus, Viscosity of silica, *J. Appl. Phys.* **92**, 7619 (2002).
- [54] The data digitalization software is Plot Digitizer <https://plotdigitizer.com/>.
- [55] J. G. Proakis, *Digital Signal Processing: Principles Algorithms and Applications* (Pearson Education India, New Delhi, 2001).
- [56] M. Parker, *Digital Signal Processing 101: Everything You Need to Know to Get Started* (Elsevier Science, Amsterdam, 2010).
- [57] R. G. Lyons, *Understanding Digital Signal Processing: Unders Digita Signal Proces_3* (Pearson Education, London, 2010).
- [58] M. L. Johnson, M. E. Blodgett, K. A. Lokshin, N. A. Mauro, J. Neuefeind, C. Pueblo, D. G. Quirinale, A. J. Vogt, T. Egami, A. I. Goldman, and K. F. Kelton, Measurements of structural and chemical order in $Zr_{80}Pt_{20}$ and $Zr_{77}Rh_{23}$ liquids, *Phys. Rev. B* **93**, 054203 (2016).
- [59] E. A. Guggenheim, The principle of corresponding states, *J. Chem. Phys.* **13**, 253 (1945).
- [60] H. E. Stanley, Scaling, universality, and renormalization: Three pillars of modern critical phenomena, *Rev. Mod. Phys.* **71**, S358 (1999).
- [61] J. C. Mauro, Y. Yue, A. J. Ellison, P. K. Gupta, and D. C. Allan, Viscosity of glass-forming liquids, *Proc. Natl. Acad. Sci. U.S.A.* **106**, 19780 (2009).
- [62] Q. Zheng, J. C. Mauro, A. J. Ellison, M. Potuzak, and Y. Yue, Universality of the high-temperature viscosity limit of silicate liquids, *Phys. Rev. B* **83**, 212202 (2011).
- [63] M. D. Demetriou, J. S. Harmon, M. Tao, G. Duan, K. Samwer, and W. L. Johnson, Cooperative Shear Model for the Rheology of Glass-Forming Metallic Liquids, *Phys. Rev. Lett.* **97**, 065502 (2006).
- [64] M. Baggioli and A. Zaccone, Explaining the specific heat of liquids based on instantaneous normal modes, *Phys. Rev. E* **104**, 014103 (2021).
- [65] A. Zaccone and M. Baggioli, Universal law for the vibrational density of states of liquids, *Proc. Nat. Acad. Sci. U.S.A.* **118**, e2022303118 (2021).
- [66] C. Stamper, D. Cortie, Z. Yue, X. Wang, and D. Yu, Experimental confirmation of the universal law for the vibrational density of states of liquids, *J. Phys. Chem. Lett.* **13**, 3105 (2022).
- [67] H. Vogel, The temperature dependence law of the viscosity of fluids, *Phys. Zeitschrift* **22**, 645 (1921).
- [68] G. S. Fulcher, Analysis of recent measurements of the viscosity of glasses, *J. Am. Ceram. Soc.* **8**, 339 (1925).
- [69] G. Tammann and W. Z. Hesse, The dependency of viscosity on temperature in hypothermic liquids, *Z. Anorg. Allg. Chem.* **156**, 245 (1926).
- [70] K. Shirai, Interpretation of the apparent activation energy of glass transition, *J. Phys. Commun.* **5**, 095013 (2021).
- [71] V. K. Ingle and J. G. Proakis, *Digital Signal Processing Using MATLAB V.4* (PWS Publishing Company, Boston, 1997).